complete neural stem cell (nsc) neuronal differentiation requires a branched chain amino acids-induced persistent metabolic shift towards energy metabolism

Francesco Bifari, Sissi Dolci, Emanuela Bottani, Annachiara Pino, Marzia Di Chio, Stefania Zorzin, Maurizio Ragni, Raluca Georgiana Zamfir, Dario Brunetti, Donatella Bardelli, Pietro Delfino, Maria Grazia Cattaneo, Roberta Bordo, Laura Tedesco, Fabio Rossi, Patrizia Bossolasco, Vincenzo Corbo, Guido Fumagalli, Enzo Nisoli, Alessandra Valerio, Ilaria Decimo

PII: S1043-6618(20)31171-3

DOI: https://doi.org/10.1016/j.phrs.2020.104863

Reference: YPHRS 104863

To appear in: *Pharmacological Research*

Received Date: 28 January 2020

Revised Date: 8 April 2020

Accepted Date: 24 April 2020

Please cite this article as: Bifari F, Dolci S, Bottani E, Pino A, Chio MD, Zorzin S, Ragni M, Zamfir RG, Brunetti D, Bardelli D, Delfino P, Cattaneo MG, Bordo R, Tedesco L, Rossi F, Bossolasco P, Corbo V, Fumagalli G, Nisoli E, Valerio A, Decimo I, complete neural stem cell (nsc) neuronal differentiation requires a branched chain amino acids-induced persistent metabolic shift towards energy metabolism, *Pharmacological Research* (2020), doi: https://doi.org/10.1016/j.phrs.2020.104863

COMPLETE NEURAL STEM CELL (NSC) NEURONAL DIFFERENTIATION REQUIRES A BRANCHED CHAIN AMINO ACIDS-INDUCED PERSISTENT METABOLIC SHIFT TOWARDS ENERGY METABOLISM

Francesco Bifari[1#], Sissi Dolci[2#], Emanuela Bottani[2,3#], Annachiara Pino[2#], Marzia Di Chio[2], Stefania Zorzin[2], Maurizio Ragni[4], Raluca Georgiana Zamfir[2], Dario Brunetti[4], Donatella Bardelli[5], Pietro Delfino[6], Maria Grazia Cattaneo[7], Roberta Bordo[1], Laura Tedesco[4], Fabio Rossi[4], Patrizia Bossolasco[5], Vincenzo Corbo[6], Guido Fumagalli[2], Enzo Nisoli[4*], Alessandra Valerio[3†], and Ilaria Decimo[2†*]*

Affiliation:

[1]Laboratory of Cell Metabolism and Regenerative Medicine, Department of Medical Biotechnology and Translational Medicine, University of Milan, Milan, Italy; [2]Department of Diagnostics and Public Health, Section of Pharmacology, University of Verona, Verona, Italy; [3]Department of Molecular and Translational Medicine, University of Brescia, Brescia, Italy; [4]Center for Study and Research on Obesity, Department of Medical Biotechnology and Translational Medicine, University of Milan, Milan, Italy, [5]Department of Neurology and Laboratory of Neuroscience, IRCCS Istituto Auxologico Italiano, Milan, Italy; [6]Department of Diagnostics and Public Health, Section of Pathological Anatomy, University of Verona, Verona, Italy; [7]Department of Medical Biotechnology and Translational Medicine, University of Milan, Milan, Italy

co-first authors
† co-last authors
* corresponding authors

*Corresponding authors:

Ilaria Decimo, PhD
Sect. of Pharmacology
Dept. of Diagnostics and Public Health
University of Verona
P.le Scuro 10, 37134 Verona, Italy
tel: +39 045 802 7509
fax +39 045 802 7452
e-mail: ilaria.decimo@univr.it

Enzo Nisoli, MD PhD
Department of Medical Biotechnology and Translational Medicine
University of Milan
via Vanvitelli, 32 - 20129, Milan, Italy

tel. +39 02 5031 6956
fax. +39 02 5031 7118
e-mail: enzo.nisoli@unimi.it

Francesco Bifari, MD, PhD
Laboratory of Cell Metabolism and Regenerative Medicine
Department of Medical Biotechnology and Translational Medicine
University of Milan
Via Vanvitelli 32, 20129, Milan, Italy
tel. +39 02 5031 6991
fax. +39 02 5031 7056
e-mail: francesco.bifari@unimi.it

RUNNING TITLE

Branched-chain amino acids-driven energy metabolic shift for neural differentiation

GRAPHICAL ABSTRACT

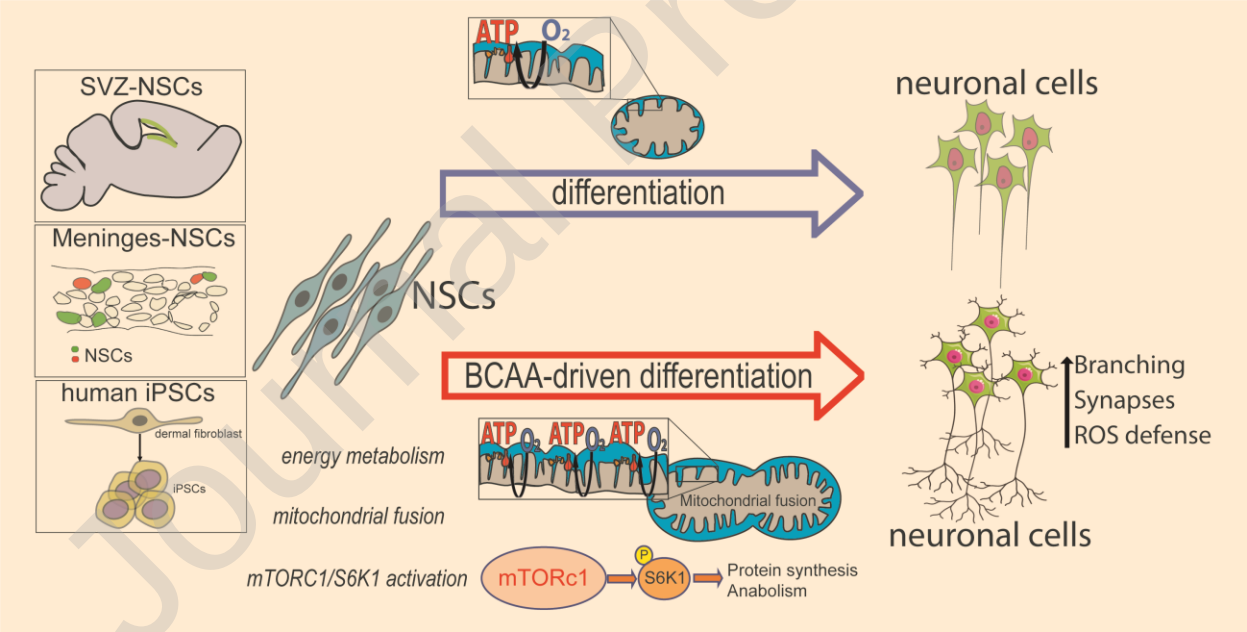

ABSTRACT

Neural stem cell (NSC) neuronal differentiation requires a metabolic shift towards oxidative phosphorylation. We now show that a branched-chain amino acids-driven, persistent metabolic shift toward energy metabolism is required for full neuronal maturation. We increased energy metabolism of differentiating neurons derived both from murine NSCs and human induced pluripotent stem cells (iPSCs) by supplementing the cell culture medium with a mixture composed of branched-chain amino acids, essential amino acids, TCA cycle precursors and co-factors. We found that treated differentiating neuronal cells with enhanced energy metabolism increased: i) total dendritic length; ii) the mean number of branches and iii) the number and maturation of the dendritic spines. Furthermore, neuronal spines in treated neurons appeared more stable with stubby and mushroom phenotype and with increased expression of molecules involved in synapse formation. Treated neurons modified their mitochondrial dynamics increasing the mitochondrial fusion and, consistently with the increase of cellular ATP content, they activated cellular mTORC1 dependent p70S6K anabolism. Global transcriptomic analysis further revealed that treated neurons induce Nrf2 mediated gene expression. This was correlated with a functional increase in the reactive oxygen species (ROS) scavenging mechanisms.

In conclusion, persistent branched-chain amino acids-driven metabolic shift toward energy metabolism enhanced neuronal differentiation and antioxidant defences. These finding offer new opportunities to pharmacological modulate NSC neuronal differentiation and to develop effective strategies for treating neurodegenerative diseases.

KEYWORDS

Neuronal Differentiation; Neural Stem Cells; human iPSC; Cell metabolism; ROS metabolism; Metabolic rewiring; mTORC1.

INTRODUCTION

Pharmacological modulation of neuronal morphogenesis and maturation has been proposed as an attractive therapeutic opportunity for the treatment of neurological diseases, including stroke, traumatic brain injury and spinal cord injury.

In the last few years, it has become clear that every cellular phenotype is characterized by a defined metabolic signature (1, 2). The brain has high energy requirements contributing to 25% of the body glucose utilization (3) and accounting for more than 20% of the body oxygen consumption. Neurons need high ATP content to support membrane remodelling, synaptic spine formation, and generation of transmembrane resting and action potential (4-6). Such high metabolic costs impose to these cells the use of the oxidative metabolism (7), which produces higher ATP yields than glycolysis. Neurons during the process of differentiation from immature precursors typically show increased oxidative phosphorylation (7-10) and such metabolic shift towards oxidative metabolism is required for neuronal differentiation. The increase of cellular ATP content, a potent allosteric inhibitor of AMPK, activates the mTOR-dependent anabolic pathway in neurons (11). Accordingly, the inhibition of oxidative metabolism impairs neuronal differentiation and drives neural stem cells (NSCs) to a proliferative and less differentiated state (12). Moreover, nutrients, including leucine, can also directly increase mTOR-dependent anabolic pathway (13). Brain damage is followed by an injury-induced activation of neural precursors characterized by increased cell proliferation and migration towards the lesion site. However, the migrated progenitors contributing to the parenchymal reaction mostly express markers of immature neural differentiation and fail to become fully differentiated neuronal cells (14, 15).

Whether a branched-chain amino acid driven persistent increase of energy metabolism in differentiating neurons may be a new strategy to enhance neuronal maturation is unknown. We previously demonstrated that supplementation with a balanced formula of essential amino acids enriched in branched-chain amino acids activate mTOR-dependent anabolic pathway, increase oxidative phosphorylation and reduce reactive oxygen species (ROS) production in different tissues (16-22). Studies on mice models of traumatic brain injury (TBI) have shown that dietary supplementation of branched-chain amino acids ameliorate cognitive impairment (23). Following pilot human studies, amino acid supplementation emerged as promising treatment options for

TBI (17, 24). In order to obtain an optimal and persistent increase in energy metabolism in differentiating neurons, we used a formulation, referred to as α5, composed of branched-chain amino acids, tricarboxylic acid (TCA) cycle intermediates, and co-factors optimized to improve mitochondrial function in different cell lines (see Table S1) (25). We tested the effect of α5 treatment on the phenotype of neuronal differentiating cells and we studied the molecular events associated. As neuronal precursors, we used both NSCs from the subventricular zone (SVZ-NSCs; sorted for the expression of prominin) and the NSCs present in meninges (M-NSCs; sorted for the expression of PDGFRß), that we have previously identified and characterized (14, 15, 26-30). To further test whether the effects of α5 were restricted to murine NSCs, or they were conserved in human neuronal differentiation, we confirmed our results on motor neurons derived from human induced pluripotent stem cells (iPSCs).

MATERIAL AND METHODS

Neural stem cell culture.

Animal housing and all experimental procedures were approved by the Istituto Superiore di Sanità (I.S.S., National Institute of Health; protocol n. 237/2016-PR and n.72/2018-PR, Italy) and the Animal Ethics Committee (C.I.R.S.A.L., Centro Interdipartimentale di Servizio alla Ricerca Sperimentale) of the University of Verona (Italy). Meninges were extracted from WT CD1 P0 pup brains, then dissociated as previously described (28, 30) and immunomagnetically sorted for PDGFRß expression (Biotinylated goat anti-PDGFRß 1:50, BAF1042; Streptavidin MicroBeads [Miltenyi], 130-048-101) according to manufacturer's instructions. Subventricular zone derived (VZ/SVZ) cells were extracted from WT CD1 P0 pup brains, then dissociated and immunomagnetically sorted for Prominin expression (mouse anti-Prominin microbeads, 1:5 [Miltenyi], 120-003-396]. PDGFRß+ meningeal-derived neural stem cells (meningeal NSCs) and Prominin+ VZ/SVZ-sorted cells (SVZ-derived NSCs) were then cultured as neurospheres as described in Bifari et al., 2009. Briefly, cells were seeded into 6-well plates (Falcon) in 3 ml of neurosphere culture medium (DMEM/F-12 GlutaMAX [Thermo Fisher Scientific], containing 2% B27 supplement [Thermo Fisher Scientific], 1% N2 supplement [Thermo Fisher Scientific], 1% penicillin-streptomycin (P/S) [Thermo Fisher Scientific], plus 20 ng/ml epidermal growth factor (EGF) [Peprotech Inc.] and 20 ng/ml basic fibroblast growth factor (bFGF) [Peprotech

Inc.]). Every 2-3 days, half of the medium (approximately 1.5 ml) was substituted with fresh NS medium. After 7-10 days, neurospheres were collected, centrifuged, mechanically dissociated to a single-cell suspension and further expanded in NS medium into T75 flasks.

Human Induced Pluripotent Stem Cells (iPSCs) generation and culture

iPSCs were obtained reprogramming skin biopsy-derived fibroblasts of two healthy donors with previous written informed consent from the participants. The CytoTune-iPS 2.0 Sendai Reprogramming Kit was used following manufacturer's instructions. The karyotype analysis confirmed that no chromosomal alterations occurred during reprogramming. The iPSCs were expanded for at least 6 passages and fully characterized for the expression of the pluripotency markers Alkaline Phospatase (ALP), TRA-1-60 and Stage-specific embryonic antigen-4 (SSEA-4) by immunocytochemistry and Sex determining region Y-box 2 (Sox2), Octamer-binding transcription factor 3 (Oct 3), Octamer-binding transcription factor 4 (Oct 4) and Homeobox protein Nanog (Nanog) by RT-PCR. The ability of iPSCs to spontaneously differentiate into the three germ layer cells was also verified further confirming their pluripotency. Cells were differentiated into motor neurons as previously described (31) for the subsequent analysis.

Neuronal differentiation protocol

Murine NSCs

We differentiated meningeal NSCs and SVZ-derived NSCs into mature neurons (M-neurons and SVZ-neurons, respectively) as previously described (30). Briefly, neurospheres were collected, centrifuged and mechanically dissociated to a single-cell suspension. Then, $1x10^5$ cells were plated into a poly-D-lysine (10 μg/ml) [Sigma-Aldrich]-coated cover slip in the differentiation medium (Neuron Chow, composed by Neurobasal Medium [Thermo Fisher Scientific] containing 2% B27 supplement, 200 mM glutamine [Thermo Fisher Scientific], 10 mM glutamate [Sigma-Aldrich] and 1% P/S plus 50 ng/ml brain-derived nerve growth factor (BDNF) [Peprotech Inc.]). The medium was changed every 2-3 days. After 10 days *in vitro* (DIV), cells were washed in PBS 1X and then fixed for 10 minutes in PFA 4% before immunostaining.

Human Induced Pluripotent Stem Cells (iPSCs)

Cells were differentiated into motor neurons as previously described (31) for the subsequent analysis. Cells were seeded at high density ($18x10^3$ cells/cm^2) for RNA and protein extraction,

and low density ($5x10^3$ cells/cm^2) for immunocytochemical analysis and Seahorse cell culture microplates.

***In vitro* cell supplementation**

Neuronal cells (SVZ-neurons, M-neurons and human iPSCs) were supplemented with a mixture (referred to as α5) composed of essential amino acids, TCA intermediates and co-factors (produced by Professional Dietetics, Italy). The mixture was added at 0.5% (w/vol) to achieve final media concentration as follows: histidine (0.10 mM), isoleucine (0.40 mM), leucine (1.19 mM), lysine (0.58 mM), methionine (30 uM), phenylalanine (60 uM), threonine (0.30 mM), tryptophan (50 uM), valine (0,44 mM), cysteine (0.13 mM), tyrosine (20 uM), thiamine (75 nM), pyridoxine (112 nM) citric acid (0.21 mM), malic acid (70 uM) and succinic acid (80 uM) (Table S1). For comparison, we tested the α1 mixture 0.5% (w/vol) having the same composition of α5, with the exception of TCA intermediates (citric, malic and succinic acid) (Table S1). To determine whether the differentiation action of these mixtures was due to their specific amino acid composition, we generated another formula with a mixture of free amino acids designed on the amino acid profile of casein, the principal protein component of rodent diets. This mixture (referred to as Cas, Table S1) was added at 0.5% (w/vol) concentration. Medium pH was adjusted at 7.4 and then Cas, α1 or α5 containing-media were filtered before being added to the specific cell culture condition. All media were changed every 2-3 days for the entire differentiation protocol (DIV 10).

Rapamycin/DMSO administration. The differentiation media of α5 treated PDGFRβ$^+$ meningeal NSCs was supplemented with 50 nM rapamycin or DMSO for 10 DIV (32). As control, untreated PDGFRβ+ meningeal NSCs receive in the differentiation media only DMSO for the same period. Cell medium was changed every 2-3 days for the entire treatment period.

Proliferation

Proliferation was quantified by incubating cells for 2 hr with 1mCi/ml [3H]-thymidine. Thereafter, cells were fixed with 100% ethanol for 15 min at 4°C, precipitated with 10% trichloroacetic acid and lysed with 0.1 N NaOH. The amount of [3H]-thymidine incorporated into DNA was measured by scintillation counting**.**

Metabolic flux assays

Matabolic flux assays of glycolysis, glucose and glutamine were done as previously described (33) by using radiolabeled tracers: 0.4mCi/ml [5-3H]-D-glucose (PerkinElmer), 0.55mCi/ml [6-14C]-D-Glucose, 0.5mCi/ml [U-14C]-glutamine.

Global transcriptomic (RNA Sequencing)

RNA from meningeal and SVZ neuronal differentiating cell (DIV 5) was extracted with TRIzol (Life Technologies). RNA quality control was performed with the Agilent 2200 Tape Station system and only RNAs with a RIN>8 were used for library preparation. Libraries for mRNA sequencing were prepared starting from 7 ng tot RNA for each sample by using the SMART-Seq v4 Ultra Low Input RNA Kit (Clontech-Takara). The SMART-Seq v4 Ultra Low Input RNA Kit for Sequencing incorporates SMART® (Switching Mechanism at 5' End of RNA Template) technology. This technology relies on the template switching activity of reverse transcriptase to enrich for full-length cDNAs and to add defined PCR adapters directly to both ends of the first-strand cDNA (34). This ensures that the final cDNA libraries contain the 5' end of the mRNA and maintain a true representation of the original mRNA transcripts. All samples were sequenced with the Illumina NextSeq 500 at an average of 27 million 75-bp single-end reads.

Quality of raw reads was checked with FASTQC (35). The raw sequenced reads were mapped according to the mouse reference transcriptome and genome (Genecode Release M20 (GRCm38.p6)) using STAR-2.5.3a(36). Mapped reads were assigned to Ensemble gene IDs with feature Counts 1.6.0 (37). Counts were imported to the *Bioconductor* package *DESeq2* 1.22.2 and normalized using the *vst* function(37). Differentially expressed genes were identified with a model that takes into account the different cell lines. Gene ontology and pathway enrichment analyses were performed with *Enrichr* web server (38) keeping up- and downregulated genes separate and considering a cut-off for $FDR < 0.05$. Gene set variation analysis was performed on *log2* normalized counts with the *GSVA Bioconductor* package 1.30.0 using custom gene sets (39). Heatmaps were generated with the *Bioconductor* package *ComplexHeatmaps* 1.20.0. The NRF2 pathway was downloaded from WikiPathways (40) and annotated using Cytoscape (41). Unless indicated, all the *p*-values refer to Wilcoxon rank-sum test.

Immunofluorescence

Cells were plated onto poly-D-lysine coated glass slides and the staining procedure was performed as previously described (42). Briefly, following fixation in 4% paraformaldehyde (PFA, [Sigma-Aldrich]), non-specific binding sites were blocked by incubation in a blocking

solution (3% fetal bovine serum, 3% bovine serum albumin, 0.3% Triton X-100 in PBS). Cells were incubated in a primary antibody solution for 1.5 hours at room temperature, washed three times with blocking solution and incubated in the proper secondary antibody solution for 1 hour. After three washes in blocking solution, slides were incubated for 10 minutes with the nuclear dye TO-PRO3 [Thermo Fisher Scientific] and mounted on glass microscope slides for confocal microscope quantification (Zeiss LSM 710 confocal microscope) [Carl Zeiss, Munich, Germany].

Primary antibodies: anti-MAP2 (rabbit, 1:200, M3696 [Sigma-Aldrich]), anti-TOMM20 (mouse, 1:200, ab56783 [Abcam]), anti-Synaptophysin (guinea pig, 1:200, 101 004 [Synaptic System]), anti-HB9 (rabbit 1:500 PA5-23407 [Invitrogen]), anti-Desmin (anti rabbit PA5-17182 [Invitrogen]), anti-AFP (mouse 1:500 MAB1369 [R&D sytems]), anti-AP (mouse ab109489 [Abcam]), anti-BIIITub (mouse 1:500 T8578 [Sigma]), anti-TRA1-60 (rabbit 1:500 41-1000[Invitrogen]), anti-SSEA-4 (mouse, 1:200 ab16287 [Abcam])

Extracellular Flux Analysis

Oxygen consumption rate (OCR) and Extracellular Acidification Rate (ECAR) were measured in adherent SVZ-neurons, M-neurons and human iPSCs with a Seahorse XFe24 Extracellular Flux Analyzer (Agilent Technologies, Santa Clara, CA). Cells were seeded at a density of $6x10^5$ cells/well in a XFe24-well cell culture microplate coated with poly-D-lysine and cultured in a 37°C incubator with humidified 5% CO_2 atmosphere for 10 days in neural differentiation protocol. The Seahorse XF DMEM Medium (Seahorse Bioscience, cat. No. 102353-100) used to perform the assay, was supplemented with 25mM Glucose, 1mM Sodium Pyruvate and 2mM Glutamine, at a pH of 7.4. OCR and ECAR were measured at baseline and after sequentially adding 1 μM oligomycin A, 1 μM of carbonyl cyanide 4-(trifluoromethoxy) phenylhydrazone (FCCP) and 1 μM of Rotenone and Antimycin A. The detailed protocol was as follows: Basal OCR: 3 cycles; each cycle consisting of 3′ Mixing, 2’ waiting and 3′ Recording; Oligomycin addition through port A: 3 cycles; each cycle consisting of 3′ Mixing, 2’ waiting and 3′ Recording; FCCP addition through port B: 3 cycles; each cycle consisting of 3′ Mixing, 2’ waiting and 3′ Recording; Rotenone and Antimycin addition through port C: 3 cycles; each cycle consisting of 3′ Mixing, 2’ waiting and 3′ Recording. Data was calculated as follows: Basal Respiration: $OCR_{BASAL} - ORC_{ROT.ANT}$; Maximum respiratory capacity: $OCR_{FCCP} - ORC_{ROT.ANT}$; ATP production (Oligomycin-sensitive respiration): $OCR_{BASAL} - OCR_{OLIGO}$. Spare Respiratory

Capacity: OCR_{FCCP} - OCR_{BASAL}. Since the inhibition of glycolysis by 2-deoxy-glucose was not performed, the basal ECAR data ($ECAR_{BASAL}$, before oligomycin injection) could not be cleared from non-glycolytic acidification; therefore, $ECAR_{BASAL}$ was considered and discussed as an index comprising glycolysis and CO_2-related acidification derived from the TCA cycle, the latter contributing up to the 42% of the ECAR in neural stem cells culture (43). The injection of oligomycin inhibits mitochondrial ATP production, and shifts the energy production to glycolysis. As such, the Glycolytic Reserve, calculated as $ECAR_{OLIGO} - ECAR_{BASAL}$ was considered as pure glycolytic index because not affected by the background. Data were normalized to the DNA content per well that was quantified with the CyQUANT Cell proliferation assay kit (Thermo Fisher Scientific, cat. No. C35007), according to the manufacturer's instructions.

Immunoblot analysis

Immunoblot analysis was performed as previously described (44). Briefly, whole proteins were extracted in RIPA buffer (Cell Signaling, #9806) and quantified using the Bicinchoninic Acid (BCA) Assay (Thermo Scientific). Samples were separated by 4-20% SDS-PAGE and electroblotted on PVDF membranes for immunodetection. After blocking, the membranes were probed by the appropriately diluted primary antibodies overnight at +4°C and subsequently incubated with horseradish peroxidase-conjugated secondary antibodies for 2 h at room temperature. Immunoblots were developed using the ECL system. Chemiluminescence-based immunostaining (ECL kit, Amersham) was performed using the following antibodies: anti-α-Tubulin 1:2000 (Santa Cruz Biotechnology, #sc-23948); anti-GAPDH 1:10000 (Abcam # ab8245); anti-DRP1 (Abcam # ab56788) at 1:1000 dilution; anti-MFN2 (Abcam # ab56889) at 1:1000 dilution; anti-OPA1 (BD Biosciences #622607) at 1:1000 dilution; anti-P-S6 (Cell Signaling #4858); anti-S6 (Cell Signaling #2217), anti-VDAC1 (Abcam #ab14734) at 1:1000 dilution; Total OXPHOS Rodent WB Antibody Cocktail (Abcam #ab110413) at 1:1000 dilution; anti-PITRM1 (Atlas #HPA006753) at 1:1000 dilution; anti-SIRT1 (Cell Signaling Technology #2028S) at 1:1000 dilution; anti-PGC-1α (Novus Biological, #NBP1-04676) at 1:1000 dilution. Secondary antibodies conjugated with HRP were from Invitrogen or Santa Cruz Biotechnology and used at 1:5000 dilution**.** Images were acquired with the use of ChemiDoc Imaging System apparatus (Bio-Rad Laboratories, Milan, Italy) and analysed with Image Lab™ software, version 6.0.1 for Windows (Bio-Rad Laboratories, Milan, Italy).

Protein synthesis (WB-SUnSET)

Protein synthesis in controls and α5 treated SVZ- and M-neurons was measured using Puromycin Dihydrochloride (Gene Spin). Briefly, cells were plated in a 24-well plate and loaded with Puromycin Dihydrochloride (1ug/mL) for 10 minutes at 37°C, 5% CO_2. Afterward, cells were lysed in RIPA Buffer with phosphatase and protease inhibitors and Western Blot analysis was performed with Ab anti-puromycin (Millipore, MAEBE434) on the cell lysates.

Image Analyses and Quantification

To evaluate the neuronal differentiation for each α5 condition, we performed immunofluorescence as described above. For every analysis described, quantifications were done with NIH ImageJ software [U.S. National Institutes of Health] (44). The positive-immunoreactive cells for each marker were determined using the ImageJ software. Data was expressed as percentage of positive cells/ total number of counted (TO-PRO3$^+$) cells. Images were acquired using a 100x oil objective [Carl Zeiss, Munich, Germany], with a 1024x1024 resolution, acquisition speed 7, and are maximum intensity projection images of 5-10 z-stack images (0.75 μm depth).

Neuronal morphology. Neuronal dendrites were analysed and quantified in blind by at least two independent observers using a custom-designed ImageJ plugin [U.S. National Institutes of Health]. Evaluation was performed on cells immunoreactive for MAP2 staining, which allowed for visible identification of neuronal dendrites. Data were expressed as mean number of branches/ MAP2+ cell, total dendrite length/ MAP2$^+$ cell and mean branch length/ MAP2$^+$ cell. Dendritic spines were counted using a custom-designed ImageJ plugin [U.S. National Institutes of Health] and dendritic spine morphology analysis was performed using the Neuron Studio software (45). Data was expressed as number/ type of spines/ 100μm MAP2$^+$ dendrite.

M-neurons treated with α5/rapamycin or α5/DMSO or DMSO were immunostained, as previously described, with MAP2 and DAPI and quantified in blind by at least two independent observers. Using ImageJ (U.S. National Institutes of Health) the total MAP2$^+$ branch area was evaluated. The mean area of branches was obtained as ratio between the total MAP2$^+$ branch area and the total number of MAP2$^+$ cells. At least 125 images per condition were analized in 3 independent experiments for a total of 375 images analyzed.

Synaptic puncta quantification. Immunoreactive Synaptophysin puncta were counted in blind by at least two independent observers using the SynapseCount (46) ImageJ plugin [U.S. National Institutes of Health].

Neuronal differentiation in motor neurons. ßIII-tubulin (Tub3) expression was analysed and quantified in blind by at least two independent observers using ImageJ plugin [U.S. National Institutes of Health]. Total nuclei were counted using a custom-designed ImageJ plugin [U.S. National Institutes of Health]. Data were expressed as percentage $Tub3^+$ area/ total nuclei.

Mitochondrial area. Mitochondrial area was measured as $TOMM20^+$ area/total $MAP2^+$ area as previously described (33). Neuronal mitochondria were counted in blind quantification by at least two independent observers using a custom-designed ImageJ plugin [U.S. National Institutes of Health].

Mitochondrial morphology analysis. At least 24 stacks of 0.75 μm each were acquired for each type of cell using a Zeiss LSM710 confocal microscope equipped with the 100X objective (for SVZ- and M-neurons) or with the 63X objective (for human cells). A region of interest (ROI) delimiting each single dendrite analysed from max projection images was selected. Images were then processed using a custom-designed ImageJ macro [U.S. National Institutes of Health] in order to obtain mitochondrial morphology data (number of fragmented, short and long mitochondria, mitochondrial area and perimeter). We classified mitochondria as "fragmented" when mitochondria were spherical (major axis equal to minor axis); "intermediate" when mitochondria presented a major axis less than ~2 μm M- and SVZ-neurons or ~10 μm for human cells; "elongated" were mitochondria in which the major axis was more than ~2 μm for SVZ- and M-neurons or ~10 μm for human cells (47, 48). "Fused" mitochondria were defined on the base of their interconnectivity score that describe the network of the mitochondria. This parameter was calculated by dividing the mean mitochondria area by the mean mitochondrial perimeter of all the particles analysed in the dendrite considered (49). Higher score for interconnectivity means higher mitochondrial "fusion". For SVZ- and M-neurons, at least 26 or 33 cells per condition were analysed respectively in at least 5 independent experiments for a total of 318 dendrites (for SVZ-neurons: total number analysed mitochondria: 2796; for M-neurons: total number analysed mitochondria: 2348). For human cells at least 24 cells per condition were analysed in at least 3 independent experiments for a total of 141 dendrites (total number analysed mitochondria: 2797).

Oxidative stress analysis

ROS scavenging in 2,3-Dimethoxy-1,4-naphthoquinone (DMNQ) treated cells was measured using 5-(6)-chloromethyl-2',7'-dichlorodihydrofluorescein diacetate (CM-H2DCFDA, Cayman Chemical) as previously described. Briefly, cells were plated in a black 96-well microplate and loaded for 30 min at 37°C in the dark with CM-H2DCFDA (10 µM). Afterwards, cells were exposed to DMNQ (50 µM) and fluorescence was assessed with a multi-plate reader with excitation and emission wavelengths of 485 and 530 nm, respectively (Victor™, PerkinElmer, Waltham, MA, USA).

Statistical analysis

As described for each methodology, $n \geq 5$ independent experiments each group with at least $n \geq 3$ technical replicates were used for statistical analysis. Differences between experimental conditions were analysed using unpaired t-Test or one-way ANOVA's followed by a Tukey post-test. A p value <0.05 was considered statistically significant. When different test was used, detailed description has been provided in the figure legends.

RESULTS

Branched-chain amino acid treatment drives persistent metabolic shift to energy metabolism in differentiating neurons

A shift towards oxidative phosphorylation is required during SVZ-NSC neuronal differentiation (7). To induce complete neuronal differentiation, we propose to obtain a persistent oxidative metabolism shift in differentiating neurons. Therefore, optimal combination of relevant metabolic precursors, known to increase oxidative metabolism, was evaluated. Specifically, we tested the effect of branched-chain amino acids, essential amino acids, TCA precursors, and cofactors on differentiating SVZ-NSCs (Table S1). Branched-chain amino acids such as leucine, isoleucine and valine, share the first enzymatic steps in their metabolic pathways that lead to an irreversible oxidative decarboxylation to coenzyme-A derivatives thus entering the Krebs cycle and promoting oxidative phosphorylation (50). Similarly, other amino acids like tyrosine, lysine, phenylalanine and tryptophan are metabolised to Acetyl-CoA (51). In addition, citrate, malate and succinate act via direct support of the Krebs cycle being relevant intermediates, and succinate also feeds the electrons to mitochondrial complex II (52), thereby sustaining oxidative phosphorylation. We treated for 6 days differentiating neurons with: a control casein-amino acid mixture (referred to as Cas), in which amino acids composition was that of casein; and a specific mixture of essential amino acids enriched in branched-chain amino acids, previously shown to increase mitochondrial function and activate mTORC1 complex (referred to as alpha1) (16) with the addition of TCA precursors, and cofactors (referred to as α5) (see Material and Methods). Notably, the addition of α5 maximally increased the OCR of differentiating neurons (Fig. S1A, B). Administration of either individual substrates or the mixture of essential amino acids without the TCA precursor and cofactors (α1) was less effective in increasing the OCR of differentiating neurons (Fig. S1A, B and data not shown). To better highlight the overall metabolic profile of the differentiating neurons, we create an Energy map (see Fig. S1C) represented as combination of the variation (z-score) of extracellular acidification rate (ECAR), an indirect measure of glycolysis, and of the oxygen consumption rate (OCR). Notably, the α5 mixture maximally increased the overall basal energy metabolism of the differentiating neurons (Fig. S1C).

To test whether the effect of α5 on the oxidative phosphorylation increase was not restricted to SVZ derived neurons (SVZ-neurons), but applicable more generally for stem cell differentiating into neurons, we tested α5 treatment in another NSC source. We recently identified neurogenic NSCs in meninges (M-NSCs) (14, 26, 29). M-NSCs showed comparable transcriptomic signature with SVZ-NSCs (14). However, the metabolic profile of M-NSCs and of M-NSC derived neurons (M-neurons) has never been assessed. We, therefore, performed metabolic flux analysis in M-NSCs and M-neurons (Fig. 1A-D). As expected, similarly to SVZ-neurons (7), we found a metabolic switch with a decrease in glycolysis and an increase in oxidative phosphorylation in M-neurons compared to M-NSCs (Fig. 1B-D).

To test the effect of α5 on neuronal differentiation, we added α5 to SVZ- and M- NSCs for the entire differentiation protocol (day *in vitro*, DIV 10) and we measured the energy metabolism of the differentiated neurons. At DIV 10, we observed a significant increase of basal oxygen consumption rate in SVZ-neurons and M-neurons (Fig. 1E-H). Accordingly, ATP production was increased in both SVZ-neurons and M-neurons exposed to α5 compared to untreated cells (Fig. 1I). We assessed the overall metabolic profile of SVZ- and M- differentiated neurons by the Energy map (see Fig. 1J). Following α5 administration, SVZ- and M-neurons shift in the upper left quadrant of the energy plot, indicating a more oxidative metabolism compared to untreated cells (Fig. 1J).

We further measured the capability of differentiating neurons to adapt their cell metabolism following metabolic stress, including the inhibition of ATP synthases (oligomycin) and the depolarisation of the inner mitochondrial membrane (FCCP). Hence, we analysed the maximal glycolytic and OXPHOS metabolic capabilities in terms of respiration arrest-induced maximal glycolytic rates (*i.e.*, glycolytic reserve) and depolarisation-induced maximal OXPHOS rate (*i.e.*, spare respiratory capacity and maximal respiration). Treatment with α5 instigated a significant increase of the maximal OXPHOS capabilities in both SVZ- and M-neurons as assessed by maximal respiration rate (Fig 1H) and spare respiratory capacity (Fig 1K). Furthermore, α5 treated neurons showed a significantly improved glycolytic reserve (Fig 1L). According to these data, α5 treated neurons appear to have higher energetic reservoir to cope with metabolic stress conditions, highlighting their increased metabolic plasticity (Fig. 1J).

Overall, these data indicate that α5 administration increased the energy metabolism and the metabolic plasticity in differentiating neurons.

Branched-chain amino acids-driven metabolic shift induces complete neuronal differentiation of both SVZ- and M- NSCs

Neuronal differentiated cells greatly modify their cellular morphology expanding dendrite and axonal branching and budding dendritic spines. To test our hypothesis that a branched-chain driven metabolic shift enhances NSC neuronal differentiation, we firstly evaluated changes in neuronal morphology of differentiated cells. At 10 DIV of neuronal differentiation, we analysed the morphology of the $MAP2^+$ differentiated cells in control and α5 conditions. Although we did not observe increase number of differentiated neurons (data not shown), we observed a statistical increase of mean branching number, mean and the total branch length in both α5-treated SVZ- and M- neurons (Fig. 2A-D). Dose response experiments by using α5 at 0.1%, 0.5% and 1% (w/vol) dilution, further indicated that the dilution of 0.5% more efficiently increase the neuronal morphology in both differentiating SVZ- and M- neurons (Fig. S2A-D). Therefore, we selected this dilution for all the experiments we performed (see Material and Methods for mixture concentration). The improved neuronal differentiation was also confirmed by the increase of $MAP2^+$ expression in α5 treated neuronal populations (Fig. S2E, F).

To further characterize the increased neuronal differentiation of α5 treated neurons, we evaluated synapse number and morphology. Synaptophysin is a synaptic vesicle protein ubiquitously expressed in every neuron and the measure of synaptophysin immunoreactive *puncta* has been considered as an estimation of synapse numbers (53). In line with the increased complexity of neuronal branching, we found that the number of synaptophysin immunoreactive *puncta* increased in α5 treated neurons compared to the controls (202.4±9.9 *vs* 374.7±23.7 and 194.0 ± 14,0 *vs* 245.8 ± 11.7 in SVZ and M-neurons, respectively, $p<0.05$; Fig. 2E, F). Dendritic spines are micron-sized protrusions along the dendritic shaft that are composed of a spine head and a thin spine neck that connects them to the dendritic shaft (54). Based on their morphology, three shape categories have been defined: thin, filopodia-like protrusions (“thin spines”), short spines without a well-defined spine neck (“stubby spines”) and spines with a large bulbous head (“mushroom spines”) (55). Spine number and morphology are correlated to neuronal maturation

(55). Stubby and mushroom spines increase in fully differentiated neuronal cells (55). We found a statistically significant increase of the fraction of more mature stubby and mushroom spines in α5 treated neurons compared to the control (Fig. 2H, S2G). The acquisition of a more stable spine morphology (*i.e.*, stubby and mushroom), further indicated that α5 treatment increased neuronal differentiation.

Overall, morphological and protein expression analysis showed that α5 treatment improved neuronal differentiation.

Global transcriptomic analysis highlights the increase in expression of oxidative phosphorylation and neural differentiation genes in α5 treated SVZ- and M-neurons

To further investigate α5 effect on neuronal metabolism and differentiation, we analysed the signature of differentiating neurons in control and α5 conditions by global transcriptomics (RNA sequencing) (Fig. 3A-D). Principal component analysis (PCA) of the RNA sequencing data confirmed that differentiated neurons treated with α5 were a separate population in particular on the first principal component (Fig. 3A). Transcriptomic analysis indicated that the most significant up-regulated genes in α5 treated populations were related to the Gene Ontology categories mitochondrial function, including the mitochondrial matrix, membrane, outer membrane and ribosomes, and neuronal differentiation, including the synapse, synapse part, synaptic and postsynaptic membrane (Fig. 3C). In particular, GSVA (Gene Set Variation Analysis) showed that α5 treated cells decreased the expression of undifferentiated genes (*i.e.* nestin, pax6, fabp7) and increased the expression of the neural differentiating ones (i.e. tubb3, dcx, map4) (Fig. 3D). In line with the improved neuronal differentiation of α5 treated populations, transcriptomic data confirmed the decreased expression of genes related to glycolysis (i.e. *hif1a, pfkfb3*) while an overall increased transcription in gene related to oxidative metabolism (i.e. *Sdha, Sdhb, Sucla2, Rpia, H6pd, Prps1 and 2, Atp5s, Atp5b, Rpe, Pgd, Pgls, Fh1, Idh2, Ogdh*) (Fig. 3B).

Overall, complementary approaches indicated that α5 treatment increased the oxidative metabolism and improved neuronal differentiation, as shown by increased branching, distribution of the synaptic marker and presence of morphologically more mature spines.

Branched-chain amino acids-driven metabolic shift activates mTORC1 and increases mitochondrial fusion in differentiated neurons

Neurons increase their cellular energy requirement to satisfy all the anabolic needs related to neuronal differentiation, including protein and membrane synthesis. Conditions of increased cellular nutrients (i.e. leucine) and energy availability (i.e. ATP content) are known to inhibit the AMPK, a major mTORC1 inhibitor that mediated catabolic pathways, and to increase mTORC1 activity, which plays a central role in regulating the anabolic processes (20, 56). During neuronal differentiation, mTORC1 complex activation promotes neural stem cell differentiation (11, 57, 58), whereas sustained activation of mTORC1 leads to a reduction of proliferative NSC in the SVZ (59). Therefore, we assessed whether the branched-chain amino acids-driven metabolic shift, which increased energy metabolism, ATP production and neuronal differentiation, was associated with an increase of mTORC1 dependent anabolism. Western blot analysis revealed that α5 treated SVZ-neurons increased mTORC1 serine/threonine protein kinase expression and the phosphorylation of its substrate p70S6 Kinase 1 (S6K1; Fig. 4A). As further confirmation of the anabolic effect of mTORC1/S6K1 signalling, we found that α5 treated neurons had increased overall protein synthesis (Fig. 4B) and expression of genes involved in mitochondrial protein translation (Fig. 4C). To assess whether neuronal differentiation requires activation of mTORC1/S6K1 anabolism, we administrated a low dose of the mTOR inhibitor rapamycin (50 nM) (32) and found that rapamycin treatment abolished the effect of the α5 on increasing neuronal differentiation (Fig. 4D).

To assess whether the metabolic shift to energy metabolism observed in α5 treated neurons was related to an increase of mitochondrial mass, we performed quantification of mitochondrial DNA (Fig. 4E) and expression of constitutive mitochondrial proteins (Fig. 4F-I). The amount of mitochondrial DNA (mtDNA) was not affected by the α5 treatment (Fig. 4E). In line with this, we didn't detect an increase of the amount of proteins related to mitochondrial biogenesis pathway PGC-1α and of its upstream regulator SIRT1 (60) (Fig. 4F). Accordingly, the amount of mitochondrial respiratory chain subunits, both nuclear- (UQCRC2, ATP5A) and mitochondrially-encoded (MT-COI) were unchanged upon α5 supplementation (Fig. 4F). Moreover, mitochondrial proteins of the outer mitochondrial membrane (VDAC1) and of the matrix (PITRM1) (61), were also unchanged in α5-treated neurons (Fig.4F). Altogether, these

data indicated that the shift towards energy metabolism was not due to an increase of mitochondrial mass or of the level of mitochondrial respiratory chain enzymes.

Differentiating neurons have a particular dependence on precise control of mitochondrial fission and fusion dynamics (62, 63). To fully sustain the metabolic shift towards oxidative phosphorylation, dendritic outgrowth, spine formation, and cell survival, differentiating neurons increase their mitochondrial fusion (62, 64). Elongated mitochondria are associated with increased oxidative phosphorylation (OXPHOS) activity and ATP production (65, 66). We, therefore, assessed the mitochondrial dynamic in differentiated neurons. Dynamin-related protein 1 (Drp1) mediates mitochondrial fission, while Mitofusin 2 (Mfn2) and Optic Atrophy 1 (Opa1) (67-69) are the main regulators of mitochondrial fusion in neurons (70). We then analysed the effect of α5 treatment on Drp1, Mfn2 and Opa1 protein expression in differentiating neurons. Treatment with α5 induced a decrease (0.83 ± 0.6.4 and 0.73 ± 0.33; $p<0.001$ and $p<0.05$ in SVZ- and M-neurons respectively) of DRP1 and an increase of MFN2 (2.69 ± 0.49 and 7.3 ± 2.2; $p<0.05$ in SVZ- and M-neurons respectively) and OPA1 (5.78 ± 1.8 and 6.6 ± 1.6; $p<0.01$ and $p<0.05$ in SVZ- and M-neurons respectively) protein expression, suggesting an increase in mitochondrial fusion events (Fig. 4G, I). Mitochondrial network and organelle lengths are determined by the balance between fission and fusion. Mitochondrial morphologies can change dramatically by shifting this balance (71). Our data indicated a significant upregulation in the total amount of OPA1 and MFN2 analysed in treated SVZ- and M- neurons; in particular, both long and short Opa1 isoforms were increased compared to untreated neurons (Fig. 4G, I). Since OPA1 long forms support mitochondrial fusion, whereas the short forms are better able to restore energetic efficiency (72), our data, together with the increase of MFN2, supported the idea that α5 supplementation is able to modulate mitochondrial dynamics through a shift to pro-fusion events in response to metabolic stimuli. Moreover, the upregulation of OPA1 and MFN2 was paralleled by a significant drop in the total amount of DRP1 upon α5 supplementation (Fig. 4G, I). Although we did not check neither the DRP1 localisation nor the phosphorylation status, the substantial decrease of DRP1 strongly suggested that the treatment with the α5 mixture also caused a downregulation of mitochondrial fission events. Therefore, we analysed the mitochondrial network (Fig. 4J-Q). Quantitative analysis showed that α5 treated neurons increased the mitochondrial length (Fig. 4K, L, O, P) and the mitochondrial fusion index calculated as interconnectivity score (Fig. 4M, Q) (49). These data suggested that α5 promoted

the formation of networks of elongated mitochondria in neuronal dendrites compared to the dispersed distribution of punctate mitochondria observed in control neurons (Fig. 4J-Q).

Overall, these data indicated that α5 treatment increased anabolism, mTORC1 activity and mitochondrial fusion in differentiating neurons associated with the increase of energy metabolism.

Branched-chain amino acids-driven metabolic shift increases antioxidant defence in differentiated neurons

Transcriptomic analysis highlighted that α5 treated cells, in addition to enhance neuronal differentiation, up-regulated the antioxidant related genes (Fig. 5A, B). Reactive oxygen species (ROS) are naturally produced by several metabolic reactions, most notably as a by-product of the ATP synthesis in mitochondria, and the management of the levels are important for cellular homeostasis (73, 74). Neurons, which greatly use oxidative metabolism, require proper antioxidant defences. Interestingly, the analysis of Gene Ontology enrichment for the molecular functions categories revealed that the most enriched activities of α5 treated samples were related to antioxidant activity (Fig. 5B). Likewise, an increased gene expression of relevant enzymes involved in antioxidant defence, including superoxide dismutase (*sod2*), heme oxygenase-1 (*hmox1*) glutathione synthase (*gss*) oxidase (*gpx1, gpx4, gpx8*) and reductase (*gsr*), was observed in α5 treated neurons (Fig. 5C). In accordance, a pathway analysis investigation, using WikiPathways library, further confirmed up-regulation of two critical pathways involved in antioxidant activity, such as glutathione metabolism and the NRF2 pathway (Fig. 5A, D). To further confirm that α5 treated neurons increased ROS scavenging mechanisms, we tested their antioxidant activity at functional level. When ROS levels were measured by CM-H2DCFDA labelling following the treatment with the ROS inducer DMNQ, α5 treated neurons shown a reduced increase in CM-H2DCFDA fluorescence intensity (Fig. 5E, F), implying an accelerated ROS detoxification. These data indicate that α5 treatment induces antioxidant properties in differentiating neurons.

Branched-chain amino acids-driven persistent oxidative metabolic shift increases mitochondrial elongation and neural differentiation in human iPSCs

The effect of branched-chain amino acids-driven increasing energy metabolism and neuronal differentiation was obtained from mouse NSCs of different brain regions (SVZ and meninges), suggesting that the observed effect is not limited to a specific cell origin. To evaluate whether the effects of branched-chain amino acids-driven metabolic shift on both energy metabolism and neuronal differentiation were also applicable on human neuronal cells, we tested and confirmed the results on iPSCs. Skin biopsy-derived fibroblasts were reprogrammed to generate pluripotent cells expressing pluripotency markers (Fig. 6A, C) and able to spontaneously differentiate into three germ layer cells (Fig. 6B). Human iPSCs were then differentiated into motor neurons (Fig. 6D) (31). During the last 6 days of neuronal differentiation, we administered α5 treatment and compared against control cells the OCR, the energy map, the mitochondrial network and neuronal differentiation. We found that α5 treated neurons derived from human iPSCs significantly increased their basal oxygen consumption (1.47 fold increase, Fig. 6E, F), maximum respiration (2.2 fold increase, Fig. 6E, G) and increased ATP production (1.34 fold increase, Fig. 6E, H). The overall metabolic profile represented in the energy map showed higher maximal respiration rate and spare respiratory capacity of neurons derived from human iPSCs treated with α5 treatment compared to control neurons (Fig. 6I, J). In this analysis no differences in glycolytic reserve were observed between α5 treated and control iPSCs-derived neurons (Fig. 6K).

We analysed the mitochondrial network (Fig. 6L, N-P) and we found that α5 treated neurons derived from human iPSCs greatly increased their mitochondrial area (Fig. 6L, O), the percentage of elongated mitochondria (Fig. 6P) and the mitochondrial fusion index, interconnectivity score (1.42 ± 0.08 control *vs* 1.74 ± 0.10 α5 treated cells; $p<0.05$), suggesting that α5 promoted the formation of networks of elongated mitochondria. Neuronal differentiating iPSCs in culture were highly dense therefore it was not possible to identify branch number and branch length for each cell. In order to describe the dendrite number and extension, we measured the area of expression of the neuronal dendrite marker ßIII-tubulin (Tub3) normalized for the total nuclei number. We found that the area of expression of Tub3 (Fig. 6M, Q) was increased in α5 treated neurons suggesting higher neuronal differentiation and dendrite extension.

This data indicated that α5 administration improved energy metabolism, mitochondrial elongation and neuronal differentiation in human differentiating iPSCs suggesting that α5 effect may be broad and can be extended to human neuronal differentiation.

DISCUSSION

In this work, we showed that a branched-chain driven metabolic shift enhances NSC neuronal maturation. Specifically, the administration of α5 treatment to differentiating neurons was able to increase energy metabolism, ATP production, antioxidant defence and neuronal maturation. Strikingly, we observed similar effect in differentiating neurons derived from NSC of different sources: murine SVZ and brain meninges, and human iPSCs. These observations suggested that the branched-chain amino acids-driven modulation of energy metabolism may be a useful approach to induce neuronal maturation, independently from the neuronal precursor origin and from differentiating conditions.

In vitro and *in vivo* experiments have shown that neurons differentiating from immature precursors require an increase of oxidative phosphorylation (7-9, 12, 75). Proliferating NSCs of the brain ventricle are highly glycolytic and switch towards oxidative metabolism while migrating to the upper cortical layers to become cortical neurons. Inhibition of glycolysis in SVZ NSCs modifies the number of differentiated neurons migrating to the cortex (75). Similarly, the inhibition of oxidative metabolism impairs neuronal differentiation driving NSCs to a more proliferative and less differentiated state (12). Our results confirmed that, together with a change in morphology, differentiating neural precursor shift their metabolism towards oxidative metabolism. To better define the relationship between metabolism and neuronal differentiation, we induced a branched-chain amino acids-driven metabolic shift in differentiating neurons. We found that this treatment increased the energy metabolism of differentiated neurons. Interestingly this analysis further revealed an increase of the metabolic plasticity of treated neurons, by means of increasing spare respiratory capacity and glycolytic reserve. This property may help the treated cells to maintain appropriate energetic metabolism in conditions of metabolic stress. Although, the overall energy metabolism can be measured by ECAR and OCR, the precise relative contribution of basal glycolysis is rather difficult to assess as far as other metabolic sources may contribute to the acidification of the extracellular medium, including the CO_2

released from TCA cycle (43) and the decarboxylation reactions catalysed by glucose-6 phosphate dehydrogenase and/or pyruvate dehydrogenase (76).

Together with the increase in energy metabolism, we found increased dendritic branching, presence of mature spine types and the amount of presynaptic vesicles, usually considered markers of SVZ- and M- neuron maturation (54).

To satisfy all the anabolic needs, differentiating neurons increase their cellular energy requirement along with protein and membrane synthesis. AMP-activated protein kinase (AMPK) is the main sensor of low cellular energy status as it is activated by high concentration of AMP and inhibited by high levels of ATP (74). On the other hand, mTOR is a central integrator of nutrient and growth factor signals that activates many biosynthetic pathways, especially protein translation (56). In the regulation of cellular metabolism, AMPK function antithetically to mTORC1. AMPK inhibits mTORC1 activity (77). ATP is a potent allosteric inhibitor of the AMPK and high cellular ATP concentration decreases AMPK activity and increases mTOR signalling (74). Similarly, amino acids, including leucine, directly activate mTORC1 complex trough a fine tuned multiprotein nutrient sensing complexes (13). During neuronal differentiation, concomitant to the increase of the oxidative metabolism, mTORC1 complex activation promotes neural cell differentiation (11, 57, 58, 78). Sustained activation of mTORC1 leads to a decrease of proliferative NSC in the SVZ (59). In addition, newly-born neurons in the olfactory bulb shows substantially higher levels of pS6K than neighbouring neurons (78). Similarly, mTORC1 activation increases dendritic complexity, synaptic formation and plasticity (58, 79-83). In line with current knowledge, we observed that α5 treatment highly enhanced (2 to 3 fold increase) both oxidative metabolism and ATP production. As expected, we confirmed that this was associated with increased mTORC1 expression and pS6K1 phosphorylation. In condition of high energy, nutrient and growth factors, mTORC1 activation stimulates biosynthetic pathways. Accordingly, we found an increase in protein synthesis and mitochondrial protein translation. Our results indicated that mTORC1 activation is required for neuronal differentiation, since its inhibition abolished the branched-chain amino acids-driven increase in neuronal branching. Other mechanisms, including mitochondrial fusion and oxidative phosphorylation may play a role in the observed effect on neuronal differentiation. Both mitochondrial fusion and oxidative phosphorylation contribute to increase energy availability that enhances mTORC1/SK6 activation. To our knowledge, these data show for the first time

that supplementation of specific nutrients can up-regulate the energy metabolism and the mTOR anabolic pathway in differentiating neurons.

Not surprisingly, the increase in dendrite branching, distribution of the synaptic marker synaptophysin and spine maturation, were associated with proper mitochondrial network modifications (9). Our data suggested that the increase of mitochondrial distribution and the metabolic shift to energy metabolism were not the consequence of increased mitochondrial mass or oxidative phosphorylation enzymes. However, differentiating neurons have a particular dependence on precise control of mitochondrial fission and fusion dynamics (62-64). In differentiating neurons, elongated mitochondrial networks are more efficient as energy producers and are capable of distributing energy also through dendrites (62, 69, 84). We found that treated SVZ- and M-neurons increased oxidative phosphorylation, mitochondrial respiration and ATP production, and modulated the amount of proteins involved in mitochondrial dynamics with the remodelling of mitochondrial network. Accordingly, α5 treatment increased neuronal mitochondrial area, mitochondrial length and synergistic up-regulate the pro-fusion and down-regulate the pro-fission proteins, thus shifting the balance of mitochondrial dynamics toward pro-fusion event. The observed increase of OPA1 (both long and short isoforms) could tight the structure of the mitochondrial cristae favouring supercomplexes assembly (85), and therefore increasing mitochondrial respiration (65, 86, 87), as we detected by OCR. Furthermore, OPA1 elongates the mitochondrial network (together with DRP1 decrease) by promoting mitochondrial fusion (72), as we showed by western blot and immunofluorescence analysis. These observations suggest that α5 effect may increase respiratory complex activities through mitochondrial re-shaping.

In this work we found that activation of mTORC1/S6K1 pathway was associated to an increase of mitochondrial fusion events. Previous work showed that mTORC1 activation has been shown to drive mitochondrial division in a 4E-BP-dependent mechanism (88). We think that the reason of the distinct effects of mTORC1 signalling activation on mitochondrial fusion may mostly reside in the different cell types studied, which are highly proliferating mouse embryonic fibroblast (88) and murine and human post-mitotic differentiated neurons (our work). The increase in ATP energy content is a necessary requirement for differentiating neurons. In this context mTORC1/S6K1 signalling activation may be a mediator of increased energy metabolism (ATP production) in neuronal cells, and therefore, required for dendrites maturation. In line with

this, it has been elegantly shown that oxidative culture conditions (as the ones that we applied) stimulate oxidative phosphorylation and mitochondrial elongation (89). More generally, mitochondrial elongation has been linked to increased oxidative phosphorylation in different cell types (90) and, recently, also through an mTORC1-mediated mechanism (91).

Interestingly, together with the increase in oxidative metabolism and mitochondrial fusion, we observed a significant functional improvement of antioxidant defences in α5 treated neurons. Neurons are highly dependent on oxygen metabolism for their function, thus requiring proper antioxidant defences. The increase in oxygen radical detoxification and the maintenance of an appropriate redox homeostasis help to protect neurons against brain ischemia (33). Furthermore, aging and neurodegenerative diseases have been shown to be associated with a loss of neuronal mitochondria and an increase of radical oxygen species damage. Both our transcriptomic (RNA sequencing) and functional data suggested that α5 treated neurons increased their antioxidant defence. Interestingly, the up-regulation of the antioxidant NRF2 pathway, observed in α5 treated neurons, may also contribute to enhance the mitochondrial fusion pattern as it increased proteasomal activity and selective degradation of the mitochondrial fission protein Drp1 (92).

Recently, the availability of specific metabolic precursors has been shown to favour neural cell differentiation. An increase of serine and cysteine pools can promote oligodendrocytes differentiation (93). Similarly, administration of branched-chain amino acid has been shown to ameliorate cognitive impairments in mice models of traumatic brain injury (20, 23). Our data showed that cellular metabolism can be modulated to increase neuronal differentiation. Following the addition of brain-chain aminoacid, TCA cycle intermediates and co-factors, neural differentiating cells increased: *i*) energy metabolism; *ii*) neuronal maturation and *iii*) neuronal antioxidant defence. We speculate that the possible mechanisms responsible of this process may involve the synergistic action of ATP production and the activation of both mTORC1 and NRF2 pathways (Figure 7).

These findings suggest that a branched-chain amino acids-driven modulation of the neuronal metabolism towards energy metabolism may be an effective approach to induce complete neural differentiation. This approach may be an exploitable therapy to improve neuronal survival, regeneration, and maturation in neurodegenerative diseases, including stroke, traumatic brain injury and spinal cord injury.

AUTHOR CONTRIBUTION

F.B., conceptualized and designed the study; performed experiments, analyzed and interpreted data, wrote the manuscript, financial support, final approval of manuscript; S.D., performed experiments, analyzed and interpreted data, wrote the manuscript, final approval of manuscript; A.P., performed experiments, analyzed and interpreted data, wrote the manuscript, final approval of manuscript; E.B., performed microscale oxygraphy experiments, analyzed and interpreted data, final approval of manuscript; M.D., performed experiments, analyzed and interpreted data, final approval of manuscript; S.Z., performed experiments, analyzed and interpreted data, final approval of manuscript; M.R., performed experiments, analyzed and interpreted data, final approval of manuscript; R.G.Z., performed experiments, analyzed and interpreted data, final approval of manuscript; D.B., performed experiments, analyzed and interpreted data, final approval of manuscript; P.D., analyzed and interpreted the RNA sequencing data, final approval of manuscript; D.B., performed experiments, analyzed and interpreted data, final approval of manuscript; MGC, performed experiments, analyzed and interpreted data, wrote the manuscript, final approval of manuscript; RB, performed experiments, final approval of manuscript; LT, performed experiments, final approval of manuscript; FR, performed experiments, final approval of manuscript; PB, performed experiments, analyzed and interpreted data with iPSCs, final approval of manuscript; VC, analyzed and interpreted the RNA sequencing data, final approval of manuscript; GF, analyzed and interpreted data, wrote the manuscript, final approval of manuscript; EN, conceptualized and designed the study; analyzed and interpreted data, wrote the manuscript, financial support, final approval of manuscript; AV, conceptualized and designed the study; analyzed and interpreted data, wrote the manuscript, financial support, final approval of manuscript; ID conceptualized and designed the study; performed experiments, analyzed and interpreted data, wrote the manuscript, financial support, final approval of manuscript.

DATA AVAILABILITY STATEMENT

The data that support the findings of this study are available from the corresponding author upon reasonable request.

CONFLICT OF INTEREST

The authors declare that the research was conducted in the absence of any commercial or financial relationships that could be construed as a potential conflict of interest.

ACKNOWLEDGMENT

We acknowledge Dr. Silvia Bassani, Neuroscience Institute (IN) CNR, Milan, Italy for her help on neuronal spine quantification, and Dr. Milena Mattioli, University of Milan, Italy for technical help with cell culture and Western blotting. Cariverona Foundation [grant number 2017-0604], Fondazione Italiana Sclerosi multipla (FISM) [grant number 2017/R/11] and financed or co-financed with 5 per mille public funding; European Union project FETPROACT-2018-2020 [grant number 824164], Italian patient association la Colonna and GALM and University of Verona [grant number DDSP-FUR-6616] are acknowledged for the support on research provided to I.D.; Fondazione Cariplo [grant number 2016-1006] is acknowledged for its contribution to E.N. and A.V; University of Milan [grant number BIOMETRA15-6-3003005-1 and PSR2018_RIVA_BIFARI] is acknowledged for the support on research provided to F.B. Fondazione Umberto Veronesi 2018-2019 is acknowledged for support to DB and EB. Department of Medical Biotechnology and Translational Medicine, University of Milan, Italy [grant number G46C18001510001] for the support on research provided to M.G.C.

REFERENCES

1. Knobloch M, Jessberger S. Metabolism and neurogenesis. Curr Opin Neurobiol. 2017;42:45-52.
2. Metallo CM, Vander Heiden MG. Understanding metabolic regulation and its influence on cell physiology. Mol Cell. 2013;49(3):388-398.
3. Attwell D, Laughlin SB. An energy budget for signaling in the grey matter of the brain. J Cereb Blood Flow Metab. 2001;21(10):1133-1145.
4. Hallermann S, de Kock CP, Stuart GJ, Kole MH. State and location dependence of action potential metabolic cost in cortical pyramidal neurons. Nat Neurosci. 2012;15(7):1007-1014.
5. Hasenstaub A, Otte S, Callaway E, Sejnowski TJ. Metabolic cost as a unifying principle governing neuronal biophysics. Proc Natl Acad Sci U S A. 2010;107(27):12329-12334.
6. Laughlin SB, de Ruyter van Steveninck RR, Anderson JC. The metabolic cost of neural information. Nat Neurosci. 1998;1(1):36-41.
7. Zheng X, Boyer L, Jin M, Mertens J, Kim Y, Ma L, Ma L, Hamm M, Gage FH, Hunter T. Metabolic reprogramming during neuronal differentiation from aerobic glycolysis to neuronal oxidative phosphorylation. Elife. 2016;5.
8. Beckervordersandforth R, Ebert B, Schaffner I, Moss J, Fiebig C, Shin J, Moore DL, Ghosh L, Trinchero MF, Stockburger C, Friedland K, Steib K, von Wittgenstein J, Keiner S, Redecker C, Holter SM, Xiang W, Wurst W, Jagasia R, Schinder AF, Ming GL, Toni N, Jessberger S, Song H, Lie DC. Role of Mitochondrial Metabolism in the Control of Early Lineage Progression and Aging Phenotypes in Adult Hippocampal Neurogenesis. Neuron. 2017;93(6):1518.
9. Steib K, Schaffner I, Jagasia R, Ebert B, Lie DC. Mitochondria modify exercise-induced development of stem cell-derived neurons in the adult brain. J Neurosci. 2014;34(19):6624-6633.
10. Martano G, Borroni EM, Lopci E, Cattaneo MG, Mattioli M, Bachi A, Decimo I, Bifari F. Metabolism of Stem and Progenitor Cells: Proper Methods to Answer Specific Questions. Front Mol Neurosci. 2019;12:151.
11. LiCausi F, Hartman NW. Role of mTOR Complexes in Neurogenesis. Int J Mol Sci. 2018;19(5).
12. Bartesaghi S, Graziano V, Galavotti S, Henriquez NV, Betts J, Saxena J, Minieri V, A D, Karlsson A, Martins LM, Capasso M, Nicotera P, Brandner S, De Laurenzi V, Salomoni P. Inhibition of oxidative metabolism leads to p53 genetic inactivation and transformation in neural stem cells. Proc Natl Acad Sci U S A. 2015;112(4):1059-1064.
13. Bar-Peled L, Sabatini DM. Regulation of mTORC1 by amino acids. Trends Cell Biol. 2014;24(7):400-406.
14. Pino A, Fumagalli G, Bifari F, Decimo I. New neurons in adult brain: distribution, molecular mechanisms and therapies. Biochem Pharmacol. 2017;141:4-22.
15. Decimo I, Bifari F, Rodriguez FJ, Malpeli G, Dolci S, Lavarini V, Pretto S, Vasquez S, Sciancalepore M, Montalbano A, Berton V, Krampera M, Fumagalli G. Nestin- and doublecortin-positive cells reside in adult spinal cord meninges and participate in injury-induced parenchymal reaction. Stem Cells. 2011;29(12):2062-2076.
16. D'Antona G, Ragni M, Cardile A, Tedesco L, Dossena M, Bruttini F, Caliaro F, Corsetti G, Bottinelli R, Carruba MO, Valerio A, Nisoli E. Branched-chain amino acid supplementation promotes survival and supports cardiac and skeletal muscle mitochondrial biogenesis in middle-aged mice. Cell Metab. 2010;12(4):362-372.
17. Valerio A, D'Antona G, Nisoli E. Branched-chain amino acids, mitochondrial biogenesis, and healthspan: an evolutionary perspective. Aging (Albany NY). 2011;3(5):464-478.

18. Tedesco L, Corsetti G, Ruocco C, Ragni M, Rossi F, Carruba MO, Valerio A, Nisoli E. A specific amino acid formula prevents alcoholic liver disease in rodents. Am J Physiol Gastrointest Liver Physiol. 2018;314(5):G566-G582.
19. Valerio A, Nisoli E. Nitric oxide, interorganelle communication, and energy flow: a novel route to slow aging. Front Cell Dev Biol. 2015;3:6.
20. Bifari F, Nisoli E. Branched-chain amino acids differently modulate catabolic and anabolic states in mammals: a pharmacological point of view. Br J Pharmacol. 2017;174(11):1366-1377.
21. Banfi S, D'Antona G, Ruocco C, Meregalli M, Belicchi M, Bella P, Erratico S, Donato E, Rossi F, Bifari F, Lonati C, Campaner S, Nisoli E, Torrente Y. Supplementation with a selective amino acid formula ameliorates muscular dystrophy in mdx mice. Sci Rep. 2018;8(1):14659.
22. Bifari F, Ruocco C, Decimo I, Fumagalli G, Valerio A, Nisoli E. Amino acid supplements and metabolic health: a potential interplay between intestinal microbiota and systems control. Genes Nutr. 2017;12:27.
23. Cole JT, Mitala CM, Kundu S, Verma A, Elkind JA, Nissim I, Cohen AS. Dietary branched chain amino acids ameliorate injury-induced cognitive impairment. Proc Natl Acad Sci U S A. 2010;107(1):366-371.
24. Sharma B, Lawrence DW, Hutchison MG. Branched Chain Amino Acids (BCAAs) and Traumatic Brain Injury: A Systematic Review. J Head Trauma Rehabil. 2018;33(1):33-45.
25. Laura Tedesco FR, Maurizio Ragni , Chiara Ruocco , Dario Brunetti , Michele O. Carruba , Yvan Torrente , Alessandra Valerio and Enzo Nisoli. A Special Amino-Acid Formula Tailored to Boosting Cell Respiration Prevents Mitochondrial Dysfunction and Oxidative Stress Caused by Doxorubicin in Mouse Cardiomyocytes. 2020;12(282):20.
26. Dolci S, Pino A, Berton V, Gonzalez P, Braga A, Fumagalli M, Bonfanti E, Malpeli G, Pari F, Zorzin S, Amoroso C, Moscon D, Rodriguez FJ, Fumagalli G, Bifari F, Decimo I. High Yield of Adult Oligodendrocyte Lineage Cells Obtained from Meningeal Biopsy. Front Pharmacol. 2017;8:703.
27. Decimo I, Bifari F, Krampera M, Fumagalli G. Neural stem cell niches in health and diseases. Curr Pharm Des. 2012;18(13):1755-1783.
28. Bifari F, Decimo I, Pino A, Llorens-Bobadilla E, Zhao S, Lange C, Panuccio G, Boeckx B, Thienpont B, Vinckier S, Wyns S, Bouche A, Lambrechts D, Giugliano M, Dewerchin M, Martin-Villalba A, Carmeliet P. Neurogenic Radial Glia-like Cells in Meninges Migrate and Differentiate into Functionally Integrated Neurons in the Neonatal Cortex. Cell Stem Cell. 2017;20(3):360-373 e367.
29. Bifari F, Berton V, Pino A, Kusalo M, Malpeli G, Di Chio M, Bersan E, Amato E, Scarpa A, Krampera M, Fumagalli G, Decimo I. Meninges harbor cells expressing neural precursor markers during development and adulthood. Front Cell Neurosci. 2015;9:383.
30. Bifari F, Decimo I, Chiamulera C, Bersan E, Malpeli G, Johansson J, Lisi V, Bonetti B, Fumagalli G, Pizzolo G, Krampera M. Novel stem/progenitor cells with neuronal differentiation potential reside in the leptomeningeal niche. J Cell Mol Med. 2009;13(9B):3195-3208.
31. Bossolasco P, Sassone F, Gumina V, Peverelli S, Garzo M, Silani V. Motor neuron differentiation of iPSCs obtained from peripheral blood of a mutant TARDBP ALS patient. Stem Cell Res. 2018;30:61-68.
32. Kang SA, Pacold ME, Cervantes CL, Lim D, Lou HJ, Ottina K, Gray NS, Turk BE, Yaffe MB, Sabatini DM. mTORC1 phosphorylation sites encode their sensitivity to starvation and rapamycin. Science. 2013;341(6144):1236566.
33. Quaegebeur A, Segura I, Schmieder R, Verdegem D, Decimo I, Bifari F, Dresselaers T, Eelen G, Ghosh D, Davidson SM, Schoors S, Broekaert D, Cruys B, Govaerts K, De

Legher C, Bouche A, Schoonjans L, Ramer MS, Hung G, Bossaert G, Cleveland DW, Himmelreich U, Voets T, Lemmens R, Bennett CF, Robberecht W, De Bock K, Dewerchin M, Ghesquiere B, Fendt SM, Carmeliet P. Deletion or Inhibition of the Oxygen Sensor PHD1 Protects against Ischemic Stroke via Reprogramming of Neuronal Metabolism. Cell Metab. 2016;23(2):280-291.

34. Zhu YY, Machleder EM, Chenchik A, Li R, Siebert PD. Reverse transcriptase template switching: a SMART approach for full-length cDNA library construction. Biotechniques. 2001;30(4):892-897.
35. Mamanova L, Andrews RM, James KD, Sheridan EM, Ellis PD, Langford CF, Ost TW, Collins JE, Turner DJ. FRT-seq: amplification-free, strand-specific transcriptome sequencing. Nat Methods. 2010;7(2):130-132.
36. Dobin A, Davis CA, Schlesinger F, Drenkow J, Zaleski C, Jha S, Batut P, Chaisson M, Gingeras TR. STAR: ultrafast universal RNA-seq aligner. Bioinformatics. 2013;29(1):15-21.
37. Love MI, Huber W, Anders S. Moderated estimation of fold change and dispersion for RNA-seq data with DESeq2. Genome Biol. 2014;15(12):550.
38. Kuleshov MV, Jones MR, Rouillard AD, Fernandez NF, Duan Q, Wang Z, Koplev S, Jenkins SL, Jagodnik KM, Lachmann A, McDermott MG, Monteiro CD, Gundersen GW, Ma'ayan A. Enrichr: a comprehensive gene set enrichment analysis web server 2016 update. Nucleic Acids Res. 2016;44(W1):W90-97.
39. Hanzelmann S, Castelo R, Guinney J. GSVA: gene set variation analysis for microarray and RNA-seq data. BMC Bioinformatics. 2013;14:7.
40. Pico AR, Kelder T, van Iersel MP, Hanspers K, Conklin BR, Evelo C. WikiPathways: pathway editing for the people. PLoS Biol. 2008;6(7):e184.
41. Shannon P, Markiel A, Ozier O, Baliga NS, Wang JT, Ramage D, Amin N, Schwikowski B, Ideker T. Cytoscape: a software environment for integrated models of biomolecular interaction networks. Genome Res. 2003;13(11):2498-2504.
42. Formaggio E, Fazzini F, Dalfini AC, Di Chio M, Cantu C, Decimo I, Fiorini Z, Fumagalli G, Chiamulera C. Nicotine increases the expression of neurotrophin receptor tyrosine kinase receptor A in basal forebrain cholinergic neurons. Neuroscience. 2010;166(2):580-589.
43. Mookerjee SA, Goncalves RLS, Gerencser AA, Nicholls DG, Brand MD. The contributions of respiration and glycolysis to extracellular acid production. Biochim Biophys Acta. 2015;1847(2):171-181.
44. Cattaneo MG, Vanetti C, Decimo I, Di Chio M, Martano G, Garrone G, Bifari F, Vicentini LM. Sex-specific eNOS activity and function in human endothelial cells. Sci Rep. 2017;7(1):9612.
45. Rodriguez A, Ehlenberger DB, Dickstein DL, Hof PR, Wearne SL. Automated three-dimensional detection and shape classification of dendritic spines from fluorescence microscopy images. PLoS One. 2008;3(4):e1997.
46. Dzyubenko E, Rozenberg A, Hermann DM, Faissner A. Colocalization of synapse marker proteins evaluated by STED-microscopy reveals patterns of neuronal synapse distribution in vitro. J Neurosci Methods. 2016;273:149-159.
47. Toyama EQ, Herzig S, Courchet J, Lewis TL, Jr., Loson OC, Hellberg K, Young NP, Chen H, Polleux F, Chan DC, Shaw RJ. Metabolism. AMP-activated protein kinase mediates mitochondrial fission in response to energy stress. Science. 2016;351(6270):275-281.
48. Nagashima S, Tabara LC, Tilokani L, Paupe V, Anand H, Pogson JH, Zunino R, McBride HM, Prudent J. Golgi-derived PI(4)P-containing vesicles drive late steps of mitochondrial division. Science. 2020;367(6484):1366-1371.

49. Wiemerslage L, Lee D. Quantification of mitochondrial morphology in neurites of dopaminergic neurons using multiple parameters. J Neurosci Methods. 2016;262:56-65.
50. Snell K, Duff DA. Branched-chain amino acid metabolism and alanine formation in rat diaphragm muscle in vitro. Effects of dichloroacetate. Biochem J. 1984;223(3):831-835.
51. Akram M. Citric acid cycle and role of its intermediates in metabolism. Cell Biochem Biophys. 2014;68(3):475-478.
52. Ackrell BA. Progress in understanding structure-function relationships in respiratory chain complex II. FEBS Lett. 2000;466(1):1-5.
53. Calhoun ME, Jucker M, Martin LJ, Thinakaran G, Price DL, Mouton PR. Comparative evaluation of synaptophysin-based methods for quantification of synapses. J Neurocytol. 1996;25(12):821-828.
54. Knott G, Holtmaat A. Dendritic spine plasticity--current understanding from in vivo studies. Brain Res Rev. 2008;58(2):282-289.
55. Bourne JN, Harris KM. Balancing structure and function at hippocampal dendritic spines. Annu Rev Neurosci. 2008;31:47-67.
56. Saxton RA, Sabatini DM. mTOR Signaling in Growth, Metabolism, and Disease. Cell. 2017;169(2):361-371.
57. Easley CAt, Ben-Yehudah A, Redinger CJ, Oliver SL, Varum ST, Eisinger VM, Carlisle DL, Donovan PJ, Schatten GP. mTOR-mediated activation of p70 S6K induces differentiation of pluripotent human embryonic stem cells. Cell Reprogram. 2010;12(3):263-273.
58. Agostini M, Romeo F, Inoue S, Niklison-Chirou MV, Elia AJ, Dinsdale D, Morone N, Knight RA, Mak TW, Melino G. Metabolic reprogramming during neuronal differentiation. Cell Death Differ. 2016;23(9):1502-1514.
59. Magri L, Cambiaghi M, Cominelli M, Alfaro-Cervello C, Cursi M, Pala M, Bulfone A, Garcia-Verdugo JM, Leocani L, Minicucci F, Poliani PL, Galli R. Sustained activation of mTOR pathway in embryonic neural stem cells leads to development of tuberous sclerosis complex-associated lesions. Cell Stem Cell. 2011;9(5):447-462.
60. Rodgers JT, Lerin C, Haas W, Gygi SP, Spiegelman BM, Puigserver P. Nutrient control of glucose homeostasis through a complex of PGC-1alpha and SIRT1. Nature. 2005;434(7029):113-118.
61. Brunetti D, Torsvik J, Dallabona C, Teixeira P, Sztromwasser P, Fernandez-Vizarra E, Cerutti R, Reyes A, Preziuso C, D'Amati G, Baruffini E, Goffrini P, Viscomi C, Ferrero I, Boman H, Telstad W, Johansson S, Glaser E, Knappskog PM, Zeviani M, Bindoff LA. Defective PITRM1 mitochondrial peptidase is associated with Abeta amyloidotic neurodegeneration. EMBO Mol Med. 2016;8(3):176-190.
62. Popov V, Medvedev NI, Davies HA, Stewart MG. Mitochondria form a filamentous reticular network in hippocampal dendrites but are present as discrete bodies in axons: a three-dimensional ultrastructural study. J Comp Neurol. 2005;492(1):50-65.
63. Rugarli EI, Langer T. Mitochondrial quality control: a matter of life and death for neurons. EMBO J. 2012;31(6):1336-1349.
64. Chen H, McCaffery JM, Chan DC. Mitochondrial fusion protects against neurodegeneration in the cerebellum. Cell. 2007;130(3):548-562.
65. Cogliati S, Frezza C, Soriano ME, Varanita T, Quintana-Cabrera R, Corrado M, Cipolat S, Costa V, Casarin A, Gomes LC, Perales-Clemente E, Salviati L, Fernandez-Silva P, Enriquez JA, Scorrano L. Mitochondrial cristae shape determines respiratory chain supercomplexes assembly and respiratory efficiency. Cell. 2013;155(1):160-171.
66. Chen H, Chomyn A, Chan DC. Disruption of fusion results in mitochondrial heterogeneity and dysfunction. J Biol Chem. 2005;280(28):26185-26192.

67. Chen H, Detmer SA, Ewald AJ, Griffin EE, Fraser SE, Chan DC. Mitofusins Mfn1 and Mfn2 coordinately regulate mitochondrial fusion and are essential for embryonic development. J Cell Biol. 2003;160(2):189-200.
68. Cipolat S, Martins de Brito O, Dal Zilio B, Scorrano L. OPA1 requires mitofusin 1 to promote mitochondrial fusion. Proc Natl Acad Sci U S A. 2004;101(45):15927-15932.
69. Zorzano A, Claret M. Implications of mitochondrial dynamics on neurodegeneration and on hypothalamic dysfunction. Front Aging Neurosci. 2015;7:101.
70. Tilokani L, Nagashima S, Paupe V, Prudent J. Mitochondrial dynamics: overview of molecular mechanisms. Essays Biochem. 2018;62(3):341-360.
71. van der Bliek AM, Shen Q, Kawajiri S. Mechanisms of mitochondrial fission and fusion. Cold Spring Harb Perspect Biol. 2013;5(6).
72. Del Dotto V, Mishra P, Vidoni S, Fogazza M, Maresca A, Caporali L, McCaffery JM, Cappelletti M, Baruffini E, Lenaers G, Chan D, Rugolo M, Carelli V, Zanna C. OPA1 Isoforms in the Hierarchical Organization of Mitochondrial Functions. Cell Rep. 2017;19(12):2557-2571.
73. Ray PD, Huang BW, Tsuji Y. Reactive oxygen species (ROS) homeostasis and redox regulation in cellular signaling. Cell Signal. 2012;24(5):981-990.
74. Garcia D, Shaw RJ. AMPK: Mechanisms of Cellular Energy Sensing and Restoration of Metabolic Balance. Mol Cell. 2017;66(6):789-800.
75. Lange C, Turrero Garcia M, Decimo I, Bifari F, Eelen G, Quaegebeur A, Boon R, Zhao H, Boeckx B, Chang J, Wu C, Le Noble F, Lambrechts D, Dewerchin M, Kuo CJ, Huttner WB, Carmeliet P. Relief of hypoxia by angiogenesis promotes neural stem cell differentiation by targeting glycolysis. EMBO J. 2016;35(9):924-941.
76. Pike Winer LS, Wu M. Rapid analysis of glycolytic and oxidative substrate flux of cancer cells in a microplate. PLoS One. 2014;9(10):e109916.
77. Gwinn DM, Shackelford DB, Egan DF, Mihaylova MM, Mery A, Vasquez DS, Turk BE, Shaw RJ. AMPK phosphorylation of raptor mediates a metabolic checkpoint. Mol Cell. 2008;30(2):214-226.
78. Baser A, Skabkin M, Kleber S, Dang Y, Gulculer Balta GS, Kalamakis G, Gopferich M, Ibanez DC, Schefzik R, Lopez AS, Bobadilla EL, Schultz C, Fischer B, Martin-Villalba A. Onset of differentiation is post-transcriptionally controlled in adult neural stem cells. Nature. 2019;566(7742):100-104.
79. Kumar V, Zhang MX, Swank MW, Kunz J, Wu GY. Regulation of dendritic morphogenesis by Ras-PI3K-Akt-mTOR and Ras-MAPK signaling pathways. J Neurosci. 2005;25(49):11288-11299.
80. Urbanska M, Gozdz A, Swiech LJ, Jaworski J. Mammalian target of rapamycin complex 1 (mTORC1) and 2 (mTORC2) control the dendritic arbor morphology of hippocampal neurons. J Biol Chem. 2012;287(36):30240-30256.
81. Zhang L, Huang T, Bordey A. Tsc1 haploinsufficiency is sufficient to increase dendritic patterning and Filamin A levels. Neurosci Lett. 2016;629:15-18.
82. Nikolaeva I, Kazdoba TM, Crowell B, D'Arcangelo G. Differential roles for Akt and mTORC1 in the hypertrophy of Pten mutant neurons, a cellular model of brain overgrowth disorders. Neuroscience. 2017;354:196-207.
83. Santos VR, Pun RYK, Arafa SR, LaSarge CL, Rowley S, Khademi S, Bouley T, Holland KD, Garcia-Cairasco N, Danzer SC. PTEN deletion increases hippocampal granule cell excitability in male and female mice. Neurobiol Dis. 2017;108:339-351.
84. Skulachev VP. Mitochondrial filaments and clusters as intracellular power-transmitting cables. Trends Biochem Sci. 2001;26(1):23-29.
85. Frezza C, Cipolat S, Martins de Brito O, Micaroni M, Beznoussenko GV, Rudka T, Bartoli D, Polishuck RS, Danial NN, De Strooper B, Scorrano L. OPA1 controls apoptotic cristae remodeling independently from mitochondrial fusion. Cell. 2006;126(1):177-189.

86. Lapuente-Brun E, Moreno-Loshuertos R, Acin-Perez R, Latorre-Pellicer A, Colas C, Balsa E, Perales-Clemente E, Quiros PM, Calvo E, Rodriguez-Hernandez MA, Navas P, Cruz R, Carracedo A, Lopez-Otin C, Perez-Martos A, Fernandez-Silva P, Fernandez-Vizarra E, Enriquez JA. Supercomplex assembly determines electron flux in the mitochondrial electron transport chain. Science. 2013;340(6140):1567-1570.
87. Civiletto G, Varanita T, Cerutti R, Gorletta T, Barbaro S, Marchet S, Lamperti C, Viscomi C, Scorrano L, Zeviani M. Opa1 overexpression ameliorates the phenotype of two mitochondrial disease mouse models. Cell Metab. 2015;21(6):845-854.
88. Morita M, Prudent J, Basu K, Goyon V, Katsumura S, Hulea L, Pearl D, Siddiqui N, Strack S, McGuirk S, St-Pierre J, Larsson O, Topisirovic I, Vali H, McBride HM, Bergeron JJ, Sonenberg N. mTOR Controls Mitochondrial Dynamics and Cell Survival via MTFP1. Mol Cell. 2017;67(6):922-935 e925.
89. Mishra P, Carelli V, Manfredi G, Chan DC. Proteolytic cleavage of Opa1 stimulates mitochondrial inner membrane fusion and couples fusion to oxidative phosphorylation. Cell Metab. 2014;19(4):630-641.
90. Yao CH, Wang R, Wang Y, Kung CP, Weber JD, Patti GJ. Mitochondrial fusion supports increased oxidative phosphorylation during cell proliferation. Elife. 2019;8.
91. Li T, Han J, Jia L, Hu X, Chen L, Wang Y. PKM2 coordinates glycolysis with mitochondrial fusion and oxidative phosphorylation. Protein Cell. 2019;10(8):583-594.
92. Sabouny R, Fraunberger E, Geoffrion M, Ng AC, Baird SD, Screaton RA, Milne R, McBride HM, Shutt TE. The Keap1-Nrf2 Stress Response Pathway Promotes Mitochondrial Hyperfusion Through Degradation of the Mitochondrial Fission Protein Drp1. Antioxid Redox Signal. 2017;27(18):1447-1459.
93. Beyer BA, Fang M, Sadrian B, Montenegro-Burke JR, Plaisted WC, Kok BPC, Saez E, Kondo T, Siuzdak G, Lairson LL. Metabolomics-based discovery of a metabolite that enhances oligodendrocyte maturation. Nat Chem Biol. 2018;14(1):22-28.

LEGENDS TO THE FIGURES

FIG. 1. α5 INDUCES PERSISTENT OXIDATIVE METABOLIC SHIFT IN DIFFERENTIATING NSCS.

(A) Proliferation analysis evaluated by 3H thymidine incorporation in M-NSCs and M-neurons showing decreased proliferation in M-neurons compared to M-NSCs. **(B-D)** Metabolic flux analysis in M-NSCs and M-neurons showing decreased glycolysis and increased glucose and glutamine oxidation in M-neurons compared to M-NSCs. For **(A-D)** n=6 independent experiments for each group (M-NSCs and M-neurons) were considered and at least 3 technical replicates for each n were considered. **(E,F)** Representative graph of OCR analysis showing that both SVZ-neurons (10 DIV) and M-neurons (10 DIV) supplemented with α5 (green line for SVZ-neurons and red line for M-neurons) display higher respiration rate compared to controls (dashed grey lines). **(G-I)** Quantitative analysis of OCR parameters in SVZ-neurons and M-neurons showing that α5 supplemented neurons display a higher basal **(G)**, maximal respiration **(H)** and ATP production **(I). (J-L)** Energy maps of the SVZ-neurons (green/grey square) and M-neurons (red/grey circle), representing basal metabolic rate and metabolic response after the inhibition of the ATP synthase with oligomycin and the administration of mitochondrial uncoupler FCCP. α5-treated cells are more poised to rely on aerobic metabolism at the basal state, have higher spare respiratory capacity (**K**) and glycolytic compensation (i.e., glycolytic reserve) (**L**) in response to oligomycin and FCCP, compared to CRL cells. Data are extrapolated from the Mitostress test; For **(G-L)** n≥6 independent experiments for each group (SVZ-neurons CRL, SVZ-neurons α5, M-neurons CRL and M-neurons α5) and 4 technical replicates for each n were considered. Data are presented as mean ± SEM. *=p< 0.05; **=p< 0.01; ***=p< 0.001.

FIG. 2. α5 INCREASES NEURONAL DIFFERENTIATION OF NSCS *IN VITRO*.

(A) Representative pictures of $MAP2^+$ SVZ-neurons and M-neurons at 10 DIV in control and α5 condition showing that α5 treated neurons display more ramified dendrites. In the white panel representative skeleton analysis of the neuronal branching. **(B-D)** Quantitative analysis of the number, medium length and total length of SVZ-neuron and M-neuron dendrites showing that $MAP2^+$ α5 treated neurons statistically increases the number, the medium length and the total length of branches in both populations. n= 6 independent experiments for each group were considered and at least 10 technical replicates for each n were considered. **(E)** Representative pictures of the expression of synaptophysin immunoreactive puncta in SVZ-neurons and M-neurons in control and α5 treated samples. **(F)** Quantitative analysis showing that α5 treated neurons express more $synaptophysin^+$ immunoreactive puncta compare to control neurons. n= 6 independent experiments for each group were considered and 3 technical replicates for each n were considered. **(G)** Representative images of SVZ-neuron and M-neuron $MAP2^+$ dendritic spine of different morphology in control and α5 treated neurons. Blue arrowheads

indicate thin spines, green arrowheads indicate stubby spines, while red arrowheads indicate mushroom spines. **(H)** Quantitative analysis showing that supplemented SVZ-neurons have more mushroom spines and supplemented M-neurons have more stubby spines, compared to the control. Quantification is represented as fold increase of specific dendritic spine type on the control (n≥6 independent experiments for each group, at least 120 spines/cell for 5 cells each experiment were considered). Images in panels **(E,G)** are maximum intensity projection of confocal z-stacks images. Scale bars: 50 μm. Data are presented as mean ± SEM. *=p<0.05; **=p< 0.01; ***=p< 0.001.

FIG. 3. GLOBAL TRANSCRIPTOME ANALYSIS SHOWS THAT α5 INCREASES OXIDATIVE METABOLISM AND NEURONAL DIFFERENTIATION GENES.

(A) Principal component analysis (PCA) of the RNA sequencing of α5 treated and untreated cell population showing that α5 treated M-neurons and SVZ-neurons (yellow ellipse) cluster together and separately from control untreated M-neurons and SVZ-neurons (grey ellipse) (8 different pool of cells were analysed). **(B)** Heatmap of gene expression highlights the presence of two clusters untreated and treated (framed by black line). The colours in the horizontal bar above the cluster colour bar indicate the nature of the analysed cells treated (orange) or untreated (grey); for the complete list of signature genes, see Table S2. The scaled normalized expression levels of neural stem cell, glycolysis, neural differentiation and oxidative phosphorylation genes is shown. **(C)** Cellular component Gene Ontology analysis showing that up-regulated genes in the α5 treated neurons are related to mitochondrial function, including the mitochondrial matrix, membrane, outer membrane and ribosomes and neuronal differentiation, including the synapse, synapse part, synaptic and postsynaptic membrane. **(D)** GSVA (Gene Set Variation Analysis) test shows a decreased expression of neural stem cell and glycolysis gene-sets after α5 treatment, while an increased expression of neural differentiation and oxidative metabolism gene-sets. For the complete list of signature genes, see Table S2. For each condition CRL and α5.

FIG. 4. α5 TREATMENT ACTIVATES MTORC1 PATHWAY AND INCREASES MITOCHONDRIAL FUSION

(A) Representative western blot analysis of mTORC1, S6Kinase 1 (S6K1), p70S6 Kinase 1 (pS6K1) of α5 treated and control (CRL) SVZ-neurons. Statistical analysis shows that α5 treated SVZ-neurons increase the phosphorylation of mTORC1 substrate p70S6 Kinase 1 (S6K1). For each condition CRL and α5 (n=6 independent experiments). **(B)** Puromycin incorporation detected by western blotting in control and α5 treated SVZ-neurons. The graph represents statistical analysis result showing that protein

synthesis is increased following α5 treatment (n=6 independent experiments). **(C)** Schematic drawing showing the pool of mitochondrial protein translation genes and mitochondrial protein synthesis genes that are up-regulated following α5 treatment (green up-regulated genes, orange down-regulated genes). **(D)** Quantitative analysis of the $MAP2^+$ branches area in M-neurons following the treatment with medium supplemented with α5/DMSO (-/+), or α5/rapamycin (+/+) or only DMSO (-/-), showing that the administration of rapamycin abolishes the effect of the α5 supplementation on increasing neuronal branches. **(E)** Quantification of the mitochondrial DNA copy number of SVZ-neurons and M-neurons in α5 treated and untreated conditions shows no differences in the amount of mitochondrial DNA. **(F)** Western blot (WB) analysis on differentiated neurons showing that ATP5A, MT-COI, UQCRC2, PGC-1α and SIRT1 do not change in α5 treated cells compare to control. **(G)** Western blot (WB) analysis on differentiated neurons, showing that the mitochondrial dynamics protein, Dynamin-related protein 1 (Drp1) mediating mitochondrial fission decreases in α5 treated differentiated neurons, while the main regulators of mitochondrial fusion Mitofusin 2 (Mfn2) and Optic Atrophy 1 (Opa1) increase in both SVZ- and M-neurons. The amount of mitochondrial proteins PTMR1, VDAC1 is unchanged. **(H)** The graphs show quantitative analysis of the western blotting described in **(F). (I)** The graphs show quantitative analysis of the western blotting described in **(G).** Treated SVZ-neurons (green bars), α5 treated M-neurons (red bars), controls (grey bars). For each condition CRL and α5, n=6 independent experiments. **(J)** Representative images showing that mitochondria of α5 treated SVZ-neurons labelled by the neuronal marker $MAP2^+$ (red) and the green-fluorescent mitochondrial stain (mito) are fused compare to mitochondria of untreated control (CRL). (**K**) Graph representing the mitochondrial length (μm) of control (grey) and α5 treated SVZ-neurons (green) showing that α5 supplementation resulted in a significant increase of the mitochondrial length in α5 treated SVZ-neurons (0.800 μμ m ± 0.07 μ,065 μ m) compared to control SVZ-neurons (0.503 μμ m ± 0.03 μμ m). SVZ-neurons=156 dendrites, 2796 mitochondria; 5 independent experiments. (**L**) Graph representing the percentage distribution of the mitochondrial length in control (grey) and α5 treated SVZ-neurons (green). (**M**) Quantitative analysis of the interconnectivity score (fusion index) showing that it statistically increases in α5 treated SVZ-neurons compared to control (0.166 ± 0.01 μm *vs* 0.123 ± 0.01 μm). (**N**) Representative images showing that mitochondria of α5 treated M-neurons labelled by the neuronal marker $MAP2^+$ (red) and the green-fluorescent mitochondrial stain (mito) are more elongated compared to mitochondria of untreated control (CRL). (**O**) Graph representing the mitochondrial length (μm) of control (grey) and treated M-neurons (red) showing that α5 supplementation resulted in a significant increase of the mitochondrial length in α5 treated M-neurons (0.548 μm ± 0.04 μm μ) compared to control M-neurons (0.380 μm μ± 0.02 μmμ). M-neurons = 152 dendrites, 2348 mitochondria; 6 independent experiments. (**P**) Graph showing the distribution of the mitochondrial length in control (grey) and α5 treated M-neurons (red). (**Q**) Quantitative

analysis of the interconnectivity score (fusion index) showing that it is statistically increased in α5treated M-neurons compared to control (0.166 ± 0.02 μm *vs* 0.103 ± 0.01 μm). Quantitative data are described as mean ± SEM. Statistical analysis was performed using unpaired t-tests. *=p<0.05; **=p< 0.01; ***p<0.001; ****p<0.0001.

FIG. 5. α5 TREATMENT INCREASES ANTIOXIDANT ACTIVITY

(A) Pathway enrichment analysis with Wiki Pathways shows that critical pathways involved in antioxidant activity, including glutathione metabolism, oxidative stress and the NRF2 pathway are up-regulated. **(B)** Gene Ontology of the molecular functions reveals that the most enriched activities of α5 treated samples were related to antioxidant activity. **(C)** Schematic drawing of mitochondria showing that α5 treated neurons increase the gene expression of relevant mitochondrial enzymes involved in the composition of the respiratory subunit complexes and in antioxidant defence including superoxide dismutase (sod2), heme oxygenase-1 (hmox1) glutathione synthase (gss), oxidase (gpx1, gpx4, gpx8) and reductase (gsr). In green the up-regulated genes and in red the down-regulated genes. **(D)** Nrf2 pathway as obtained from Wiki Pathways was drawn with Cytoscape. Genes boxes were coloured according to the log2FC values, from blue (low) to red (high). **(E-F)** Left: graph represents ROS levels measured by relative increase in CM-H2DCFDA fluorescence (percentage of the fluorescence value in control neurons) over time after administration of DMNQ to differentiating SVZ-neurons **(E)** and M-neurons **(F)** at 7 DIV. Right: Slope values of the curves shown left (the lower the slope, the larger the ROS scavenging capacity). α5 treated SVZ-neurons (green line) and M-neurons (red line) show a reduced increase in CM-H2DCFDA fluorescence intensity implying accelerated ROS detoxification. For each condition CRL and α5 n=6 independent experiments, linear regression analysis was used to determine the slopes. Statistical differences between slopes were calculated by using the Analysis of Covariance (ANCOVA) test. Data are presented as mean ± SEM. *=p<0.05; **=p< 0.01; ***=p< 0.001.

FIG. 6. α5 TREATMENT DRIVES PRESISTENT OXIDATIVE METABOLIC SHIFT AND INCREASES, MITOCHONDRIAL DISTRIBUTION AND NEURAL DIFFERENTIATION IN HUMAN IPSCS

(A) Immunostaining showing positivity for the expression of pluripotency markers Alkaline Phosphatase (AP, red), Tra-1-60 (green) and Stage-specific embryonic antigen-4 (SSEA-4, red) in human iPSCs-derived neurons. Nuclei are stained with DAPI (blue). Scale bar, 20 μm. **(B)** *In vitro* iPSC differentiation displaying immunoreactivity for mesodermal (desmin, green) endodermal (AFP, red) and ectodermal (ßIII-tubulin, green) germ layer markers. Nuclei are stained with DAPI (blue). Scale bar: 10 μm. **(C)** RT-PCR showing the expression of pluripotency-associated genes Sex determining region Y-box 2 (Sox2),

Octamer-binding transcription factor 3/4 (Oct3/4) and Homeobox protein Nanog (Nanog). **(D)** *In vitro* iPSC differentiation into motor neurons expressing the motor neuron marker HB9 (red). **(E)** Seahorse analysis of OCR parameter showing that human iPSCs-derived neurons supplemented with α5 (red) displayed a higher respiration rate compared to controls (light blue). **(E-F)** Graphs showing that α5 supplemented human iPSCs-derived neurons displayed a higher basal **(F)** and maximal respiration **(G)**, accompanied by an increased ATP production **(H) (**n=6 independent experiments). **(I)** Energy map of human iPSCs-derived neurons, representing basal metabolic rate metabolic response after the inhibition of the ATP synthase with oligomycin and the administration of mitochondrial uncoupler FCCP. α5-treated human iPSCs-derived neurons have higher energetic metabolism compared to untreated cells at the basal state, display higher spare respiratory capacity (**J**), and similar glycolytic compensation (glycolytic reserve) in response to the blunt of mitochondrial ATP production **(K).** Data are extrapolated from the Mitostress test; see suppl. **(L)** Immunostaining of human iPSCs-derived neurons for the mitochondrial marker Tomm20. Nuclei are stained with DAPI (blue). Scale bar: 20 µm. **(M)** Immunostaining of human iPSCs-derived neurons for ßIII-tubulin (Tub3, green). Nuclei are stained with DAPI (blue). Scale bar: 10 µm. **(N)** Immunostaining of human iPSCs-derived neurons for the mitochondrial marker Tomm20 (grey in the left panel and red in the right panel) and ßIII-tubulin (Tub3, green). Scale bar: 10 µm. **(O)** Graph representing the percentage of Tomm20 expression area normalized for ßIII-tubulin expression area**.** The percentage of Tomm20 coverage was increased compared to CRL. (**P**) Graph representing mitochondria percentage classification on the basis of their length among the total quantified mitochondria showing that the percentage of elongated mitochondria statistically increases following α5 treatment while the intermediated one decreases **(Q)** Graph represents the fold-increase of α5 treated samples compared to control (CRL) of ßIII-tubulin expression area normalized for the total nuclei number**.** The expression area of Tub3 was increased compared to CRL suggesting higher neuronal differentiation and dendrite extension. Data are presented as mean ± SEM. *=p<0.05; **=p< 0.01; ***=p< 0.001, ****=p< 0.0001. For immunostaining quantification at n=6 independent experiments and at least 6 technical replicates for each n were considered. Scale bars are 50µm **(A, B, D)**.

FIG. 7. SCHEMATIC REPRESENTATION OF THE POTENTIAL MECHANISMS OF ACTION OF BRANCHED-CHAIN AMINOACIDS ON NEURONAL DIFFERENTIATION

Scheme representing the potential mechanisms of action of α5 treatment on differentiating neurons. α5 (yellow box) may increase the overall energy metabolism (light orange box) that include tricarboxylic acid cycle (TCA) cycle flux through anaplerotic reactions (amino acids breakdown), oxidative metabolism, and mitochondrial fusion. Elongated mitochondria are associated with increased oxidative phosphorylation activity and ATP production. The increase in ATP cellular content activates mTORC1/S6K1 and reduces AMPK activity, a major inhibitor of mTORC1. Amino acids contained in

α5, especially branched-chain amino acids (valine, leucine and isoleucine) are known nutrient sensors that directly activate mTORC1/S6K1 anabolic activity. The increase in oxidative metabolism and oxygen consumption may increase the Reactive Oxygen Specie (ROS) content that in turn can activate the antioxidant NRF2 pathway. Moreover, we observed that α5 treatment increased the metabolic plasticity, which is oxidative and glycolytic reserve of the differentiating neurons. The improved mTORC1/S6K1 anabolic activity increases protein synthesis and it is instrumental for the increase of neuronal differentiation. This, together with the increase in metabolic plasticity and antioxidant defence, may contribute to enhance neuronal differentiation.n.

Figure 1

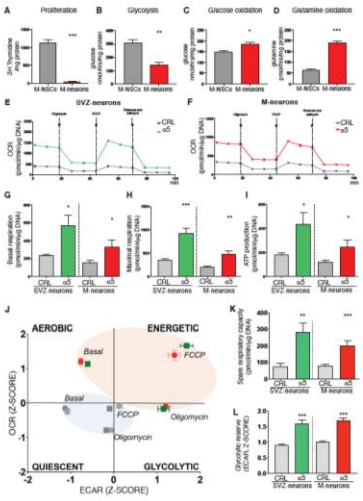

Figure 2

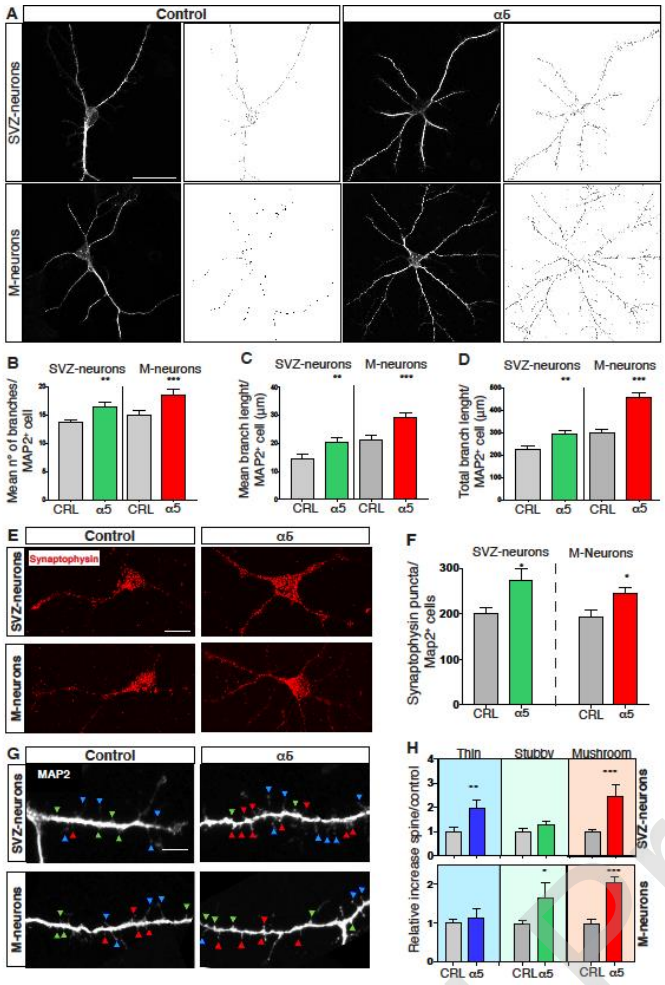

Figure 3

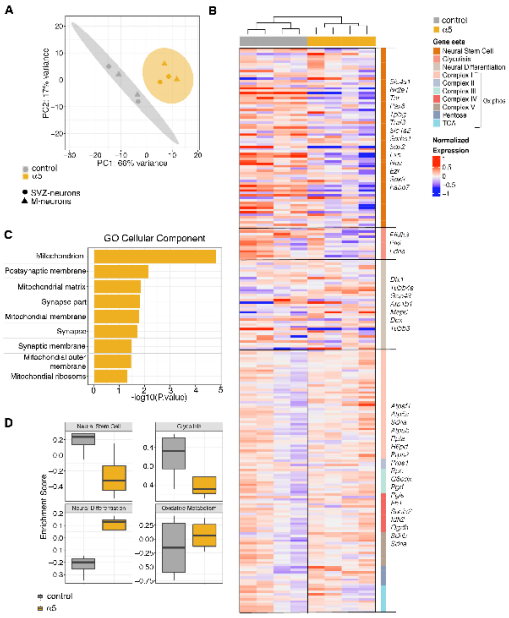

Figure 4

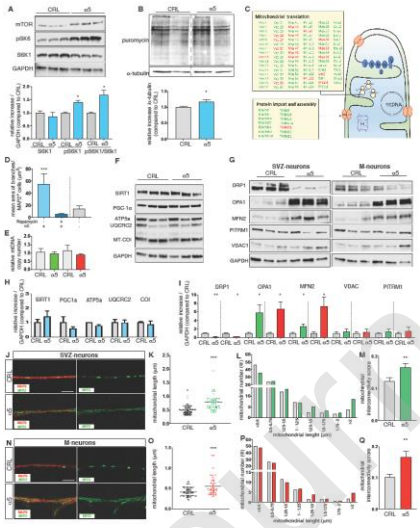

Figure 5

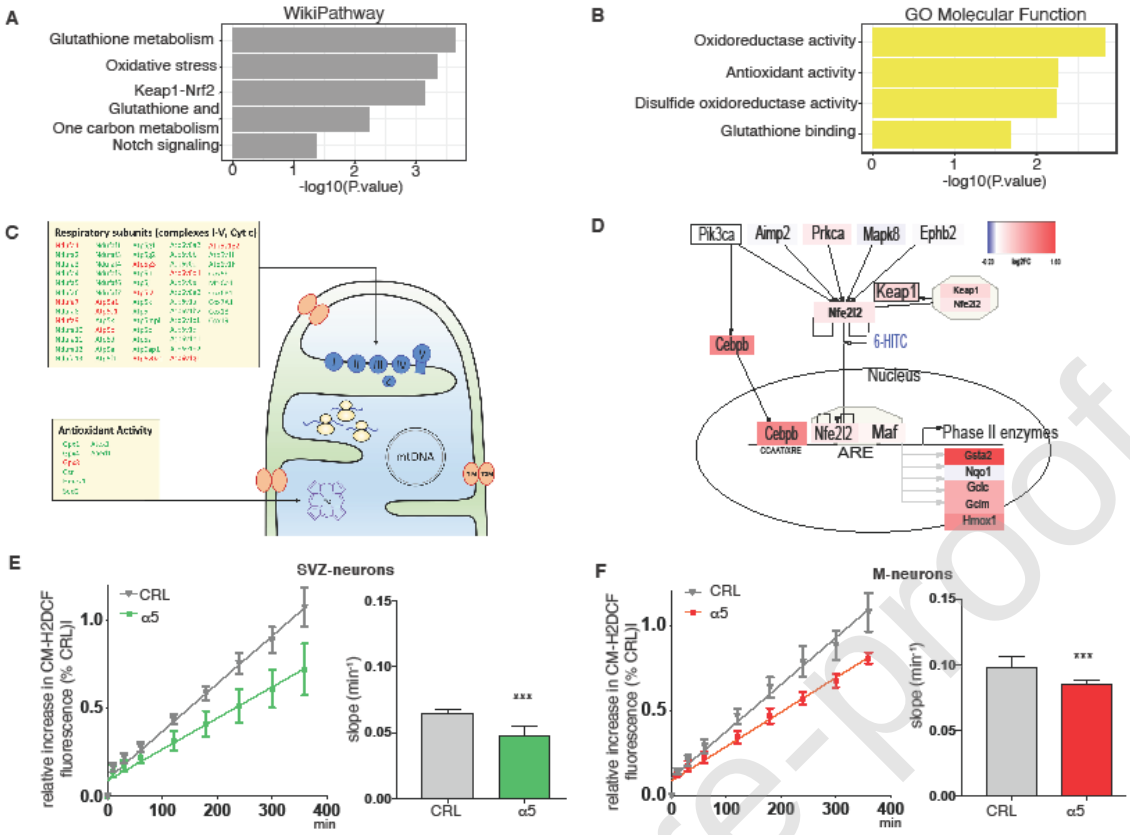

Figura 6

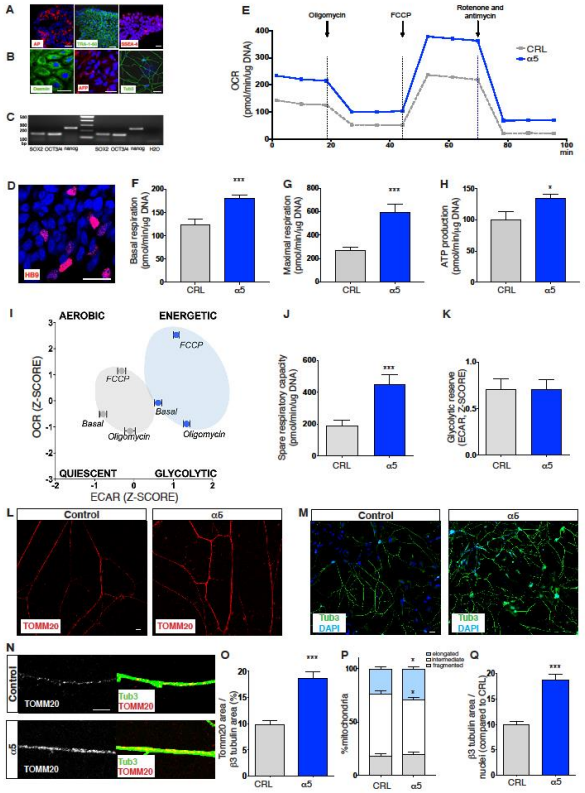

Figure 7